Hydrothermal solution calorimetry in acidic aqueous solutions and revisiting the standard partial molal thermodynamic properties of Nd^{3+} from 25 to 300 °C

Revision 2

Yerko Figueroa Penarrieta*[1,2], Alexander P. Gysi[1,2]

[1] New Mexico Bureau of Geology and Mineral Resources, New Mexico Institute of Mining and Technology, 801 Leroy Place, Socorro, NM 87801, USA

[2] Department of Earth and Environmental Science, New Mexico Institute of Mining and Technology, 801 Leroy Place, Socorro, NM 87801, USA

* Corresponding author: e-mail, yerko.figueroapenarrieta@student.nmt.edu

Tel: +1 575-835-5754

To be submitted to GCA, *for the Special Issue "Hydrothermal Geochemistry and Beyond: A Tribute to Terry M. Seward"*

Keywords: rare earth elements; calorimetry; hydrothermal; speciation; thermodynamics

ABSTRACT

The mobility of rare earth elements (REE) can be predicted in aqueous fluids using geochemical modeling but the accuracy of these models strongly depends on the availability of robust thermodynamic properties for the REE aqueous species. The REE^{3+} aqua ions are important in the derivation of the formation constants of all the major REE complexes including the chloride, sulfate, and fluoride species which predominate in many hydrothermal-magmatic systems. However, the thermodynamic properties of the REE^{3+} aqua ions are still commonly derived from the Helgeson-Kirkham-Flowers (HKF) equation of state parameters tabulated several decades ago. The standard state thermodynamic properties at reference conditions (25 °C and 1bar) and their extrapolations to high temperature need to be verified, if not revised, based on hydrothermal experiments. In this study, the enthalpy of solution was measured for synthetic Nd hydroxide from 25 to 150 ºC to retrieve the standard partial molal thermodynamic properties of Nd^{3+} as a function of temperature. The experiments were conducted in aqueous perchloric acid based solutions with starting pH of 2 and varying ionic strength (0.01 to 0.09 mol/kg $NaClO_4$). The standard partial molal enthalpy of formation ($\Delta_f H°$) of Nd^{3+} derived from the experimental study displays differences of up to 10 kJ/mol compared to the enthalpy values derived from the HKF equation of state in the studied temperature range. These inaccuracies are resolved by adjusting the standard partial molal Gibbs energy of formation ($\Delta_f G°$) of Nd^{3+} at 25 °C and 1 bar from -672.0 to -679.7 kJ/mol. The heat capacity function ($C_p°$) derived between 25 and 150 ºC can be described by: $C_p° = a_0 + a_1 \cdot T + a_2 \cdot T^{-2}$, with a_0 = 1256, a_1 = -2.68, a_2 = $-55.56 \cdot 10^6$ and T in Kelvin. A set of recommended thermodynamic properties is provided for the Nd^{3+} aqua ions and corrections are

provided for the chloride and fluoride species to remain internally consistent with the experimentally derived properties. These results allow predicting accurately the solubility of monazite between 25 and 300 ºC. Before these corrections, the properties for the Nd^{3+} aqua ions derived from the HKF parameters resulted in up to ~1.5 orders of magnitude lower monazite solubility than determined experimentally. Therefore, a revision of the REE^{+3} aqua ions properties is necessary to accurately predict the mobility of REE in hydrothermal acidic solutions.

1. INTRODUCTION

The rare earth elements (REE) are important for society due to their role in the high-tech and green-technology industries, and their use in permanent magnets, catalysts, energy efficient lights, and electronics (Long et al., 2012; Van Gosen et al., 2017; Goodenough et al., 2018; Dushyantha et al., 2020; Liu et al., 2020). In natural geologic system, hydrothermal aqueous fluids play an important role in the transport and fractionation of REE during the formation of critical mineral deposits (Williams-Jones et al., 2000; Gysi and Williams-Jones, 2013; Gysi et al., 2016; Beland and Williams-Jones, 2021). Accurate thermodynamic data for the REE aqueous species are needed because our understanding of the underlying processes that control the mobility of REE in these magmatic-hydrothermal systems largely relies on combining field observations with thermodynamic modeling (Williams-Jones et al., 2012; Gysi and Williams-Jones, 2013; Migdisov and Williams-Jones, 2014; Migdisov et al., 2016; Perry and Gysi, 2018; Pan et al., 2024).

The thermodynamic properties of many REE aqueous species have not yet been determined at hydrothermal conditions, particularly the REE^{3+} aqua ions, the REE hydroxyl, and the REE carbonate complexes (Migdisov et al., 2016); a few studies have investigated the properties of the Nd hydroxyl species (Wood et al., 2002), and the stability of the REE carbonate complexes (Louvel et al., 2022; Nisbet et al., 2022) at elevated temperature. Hydrothermal REE phosphate solubility experiments conducted in perchloric acid based solutions between 100 and 250 °C (Gysi et al., 2015, 2018; Van Hoozen et al., 2020; Gysi and Harlov, 2021) indicate that the thermodynamic properties of the REE^{3+} aqua ions and hydroxyl complexes need to be revised because thermodynamic predictions do not match the experimental observations. A thermodynamic optimization study by Pan et al. (2024) further concludes that the standard Gibbs energy of formation ($\Delta_f G°$) of the REE^{3+} aqua ions needs to be adjusted by ~2-10 kJ/mol to match the experimental solubility data for monazite, rhabdophane, and xenotime between 25 and 300 °C.

The REE^{3+} aqua ions play an important role in deriving the formation constants of most REE-ligand complexes (e.g., $REE^{3+} + Cl^- = REECl^{2+}$), including the chloride, fluoride, and sulfates species generally retrieved from hydrothermal solubility experiments (e.g. Migdisov et al., 2009, 2016). The thermodynamic properties of the REE^{3+} aqua ions are commonly calculated at elevated temperatures from the Helgeson-Kirkham-Flowers (HKF) equation of state parameters (Helgeson et al., 1981; Tanger and Helgeson, 1988; Shock and Helgeson, 1988; Shock et al., 1992), which were implemented into the slop98.dat thermodynamic database in the program SUPCRT92 (Johnson et al., 1992) several decades ago (Haas et al., 1995; Shock et al., 1997; Sverjensky et al., 1997). However, these thermodynamic properties

are rarely scrutinized, and thus, the accuracy of the predicted species stabilities are currently unknown.

In this study, hydrothermal solution calorimetric experiments were conducted between 25 and 150 °C to measure the enthalpy of solution of solid Nd hydroxide in perchloric acid based aqueous solutions with a starting pH of 2. The experimental data are used to derive the standard partial molal enthalpy of formation of the Nd^{3+} aqua ion as a function of temperature and the corresponding heat capacity function. A robust set of recommended thermodynamic properties is provided to accurately predict the solubility and speciation of Nd in acidic hydrothermal aqueous fluids.

2. METHODS

2.1. Materials

Crystalline Nd hydroxide [$Nd(OH)_3(s)$] was synthesized following a similar hydrothermal synthesis method outlined by Diakonov et al. (1998a, 1998b). About 5 g of $Nd_2O_3(s)$ (Alfa Aesar, 99.99% purity) was first mixed with 25 mL of Milli-Q water (18.2 MΩ-cm), and the solution was then transferred to a batch-type reactor (Parr 4744, Teflon-lined stainless steel). The head space of the reactor was first purged with ultra high purity N_2 gas, then closed and the solution was equilibrated at 250 °C for up to 21 days. This resulted in the precipitation and recrystallization of solid Nd hydroxide according to the chemical reaction $Nd_2O_3(s) + 3H_2O(aq) \rightarrow 2Nd(OH)_3(s)$ (Baes and Mesmer, 1981). The furnace temperature was recorded using a K-type thermocouple (Omega KQXL-18U-12) and a data-logger (Omega EL-USB-

105 TC). The reactor was quenched in a water bath in less than 20 min and the slurry oven dried at
106 75 °C for 24 hours at the end of each synthesis cycle. The solid Nd hydroxide powder was
107 characterized using X-ray diffraction (XRD) and Raman spectroscopy. Subsequently, the
108 powder was stored in a desiccator until used in an experiment.

109 The perchloric acid based experimental starting solution used in the solution
110 calorimetric experiments were prepared using trace metal grade perchloric acid (Fisher
111 Scientific), which was added drop wise to 500 ml of Milli-Q water until a pH of 2.00 ±0.02
112 was measured at ambient temperature (20 ±2 °C). The pH measurements were used to
113 determine the initial ClO_4^- concentration of the starting solution; perchloric acid was used
114 because ClO_4^- does not readily form complexes in aqueous solutions with REE^{3+} at below
115 ~250−300 °C and has a negligible complexation with most metal ions at low molalities (Hakin
116 et al., 2003). A pH of 2 was selected to limit the formation of REE hydroxyl complexes and to
117 increase the dissolution of the Nd hydroxide powders (Migdisov et al., 2009; Gysi et al., 2018).
118 Solid sodium perchlorate (Sigma-Aldrich, 99.99% purity) was used to prepare a series of
119 experimental $NaClO_4$-$HClO_4$-H_2O solutions of varying initial ionic strength. Sodium chloride
120 (Puratronic™ metal basis, 99.998 %) was used in the test experiments to determine the overall
121 accuracy of the calorimetric experiments.

122

123 **2.2. Experimental methods**

124 Hydrothermal solution calorimetric experiments were conducted in a Setaram Model C-80
125 calorimeter with a reversal mechanism (Fig. 1a). The methodology used was further developed

here based on the study by Coulier and Tremaine (2014). Experiments were conducted between 25 and 150 °C to measure the heat of solution of $Nd(OH)_3(s)$ in the perchloric acid based experimental starting solutions with a pH of 2 and an ionic strength of 0.01.

The calorimetric instrument is based on the Tian-Calvet heat flow principle (Calvet and Prat, 1963) and consists of two identical tubular wells in a thermo-stated aluminum block. Each well is surrounded by 3-D thermopiles (flux-meters) designed to measure the heat flux in each of them; one flux-meter measures the heat flow from/to the experimental sample and the other from/to an inert reference. The difference between the cell sample and the cell reference allows the measurement of all heat evolved or adsorbed, including radiation, convection or conduction. Two identical 5 ml Hastelloy C-276 reaction cells (Setaram, S60/58313) fit into these cylindrical thermopiles, i.e. one acts as the container for the experimental sample and the other acts as the reference with a blank solution.

Each Hastelloy reaction cell contains two isolated compartments (Fig. 1b) which permit mixing a solid and a liquid sample using the calorimeter reversal mechanism. A typical experiment consists of first loading the sample cell with ~35 mg solid Nd hydroxide powder, closing the lower cell with a lid and adding 3 g of the perchloric acid based experimental starting solutions in the top compartment. The mass of solid was carefully chosen based on a series of preliminary experiments at 150 °C by varying the initial $Nd(OH)_3(s)$ powder mass from 15 to 45 mg in the solid compartment. These tests indicate that ~35 mg or more of $Nd(OH)_3(s)$ is needed to reach a rapid dissolution and steady state during an experiment. The reference cell is loaded only with Milli-Q water in the top compartment. The calorimeter assembly is then heated at 2 °C/min to reach the desired experimental temperature followed by

a stabilization time of 5 h. After reaching thermal equilibrium, the reversal system is turned on to rock the calorimeter back and forth with a rotational period of ~10 s. The Nd hydroxide dissolution is allowed to proceed for an hour according to the following reaction,

$$Nd(OH)_3(s) + 3H^+ \rightleftharpoons Nd^{3+} + 3H_2O(aq) \quad (1)$$

The end of the reaction is determined based on integration of the measured heat flow curve and the baseline signal which needs to be the same at the beginning and end of each experiment. At the end of an experiment, the calorimeter is cooled to room temperature and the sample reaction cell is opened to retrieve a 2 g aliquot of the experimental solution filtered through a 0.22 μm cellulose acetate filter. This solution is subsequently diluted with 2% HNO_3 (Fisher Scientific; trace element grade) blank solution for further analysis of total dissolved Nd concentrations using inductively coupled plasma optical emission spectroscopy (ICP-OES). The total moles of dissolved Nd hydroxide was used to normalize the measured enthalpy of solution to J/mol. The Hastelloy reaction cells are both cleaned in-between experiments using a 2% HNO_3 blank solution in an ultrasonic bath for 5 min followed by another 5 min rinse with Milli-Q water.

Replicate experiments are used to test the reproducibility and uncertainty of the method assuming a steady-state Nd concentration after solid dissolution and equilibration with the aqueous solution. Three to six replicate experiments were conducted at each temperature ranging from 25 to 150 °C to evaluate the uncertainty of the method. Additional three to six replicates were performed at selected temperatures at various ionic strengths (0.01, 0.05, and 0.09 mol/kg $NaClO_4$). Blank experiments were conducted using perchloric acid based

169 experimental starting solutions in the fluid compartments and leaving the lower compartment
170 with the lid empty to measure additional possible heat contributions to the measured heat flow
171 signal (Djamali and Cobble, 2009; Coulier and Tremaine, 2014).

172 A series of NaCl dissolution test experiments were conducted to verify the accuracy of
173 the Setaram C-80 calorimeter. The approach adopted is similar to the one presented by Coulier
174 and Tremaine (2014). The reaction sample cell is loaded with 9 to 42 mg NaCl powder, the
175 compartment closed, and the top compartment is loaded with 3 g of Milli-Q water. The heat of
176 solution was measured at varying ionic strength using 0.05 to 0.24 mol/kg NaCl, depending on
177 the initial amount of NaCl powder loaded in the cell.

178

179 **2.3. Analytical**

180 The synthetic $Nd(OH)_3(s)$ powders were characterized using a Panalytical X'Pert Pro XRD
181 instrument at the New Mexico Bureau of Geology and Mineral Resources, New Mexico
182 Institute of Mining and Technology. The analyses with Cu-Kα radiation were conducted with
183 2θ scanning angles ranging between 5° and 70° in 0.02° steps. The samples were prepared by
184 dry-pressing powders for randomly oriented crystals and mounted on amorphous silica plates
185 which are rotated during analysis. Phase identification was first evaluated by matching peaks
186 positions, *d*-spacing and relative intensities with the ICSD database (Belsky et al., 2002) in the
187 software HighScore Plus. Unit cell refinement was carried out using the MAUD software
188 (Lutterotti, 2000) assuming a hexagonal ($P6_3/m$) crystal system (Beall et al., 1976).

189 Raman spectroscopy was performed using a Horiba LabRam HR Evolution confocal

190 microscope at the Raman Microscopy Laboratory, New Mexico Bureau of Geology and
191 Mineral Resources, New Mexico Institute of Mining and Technology. The instrument is
192 equipped with a 532 nm excitation Nd:YAG laser. The $Nd(OH)_3(s)$ powders were analyzed
193 using an Olympus 50x LWD objective (NA=0.5; WD =10.6 mm). The spectra was collected
194 from 40 cm^{-1} to 4500 cm^{-1} using the 1800 grooves/mm grating with a spectral resolution better
195 than 0.5 cm^{-1}. Spectra were collected at 25% laser power, 15 s acquisition time and 5
196 accumulations. The Raman spectra were calibrated using a first-order Si line at 520.7 cm^{-1}
197 (silicon wafer).

198 The pH of the perchloric acid based experimental starting solutions was measured
199 using a Metrohm 913 pH meter equipped with a combined pH/temperature glass electrode
200 (6.0260.010 Unitrode Metrohm). The electrode was calibrated with three buffer solutions
201 (Fisherbrand; pH of 1.68, 4.01 and 7.00) with a measurement precision of 0.01 pH units and an
202 accuracy of ± 0.02.

203 The quenched experimental solutions were analyzed for total dissolved Nd
204 concentrations using an Agilent 5900 ICP-OES at the Analytical Chemistry Laboratory in the
205 New Mexico Bureau of Geology, New Mexico Institute of Mining and Technology. The
206 standards and samples were spiked in-line with indium (SCP Science, NIST traceable) as an
207 internal standard for drift corrections. The calibration of the ICP-OES was conducted using six
208 standards with Nd concentrations ranging from 0.3 to 5.0 ppm. The Nd standard was prepared
209 from dilution of a 1000 µg/mL Nd stock standard (Inorganic Ventures CGND1, 1000 ±4 ppm)
210 with a 2% HNO_3 (Fisher Scientific, trace element grade) blank. The analytical precision was
211 assessed by triplicate analysis and continued calibration verification after each eight samples,

resulting in a precision of better than 2% in the considered concentration range. The limit of detection was determined from multiple 2% HNO_3 blank solution analysis yielding a standard deviation (3σ) of 2 ppb for Nd.

2.4. Data treatment

2.4.1. Retrieval of the enthalpy of solution

The heat (q) released or absorbed in the calorimetric experiments is defined by the heat flow rate (Φ_r in mW) exchanged between the calorimeter and the sample integrated over time (t in seconds) to retrieve the observed heat of solution (q_{obs} in J) according to,

$$q_{obs} = \int_{t_1}^{t_2} \phi_r(t) \cdot dt \quad (2)$$

The q_{obs} value contains several heat source contributions that are subtracted to determine the heat of solution (q_{sol}) of the crystalline Nd hydroxide powder (Eq. 1) defined by,

$$q_{sol} = q_{obs} - q_{blk} \quad (3)$$

The heat measured in a blank experiment (q_{blk}) includes any external heat sources to be considered (Djamali and Cobble, 2009; Arcis et al., 2014) such as the heat of vaporization (q_{bulb}) and heat of condensation (q_{vp}) during opening of the solution-free cell compartment, and the mechanical heat generated by the rotation of the calorimeter (q_{th}). Coulier and Tremaine (2014) critically assessed those external heat sources using a theoretical approach and considering the temperature of the experiments with minimal heat contributions at temperatures <200 °C. The contribution of q_{blk} in our experiments resulted in corrections

ranging between -0.8 mJ at 25 °C and -46.2 mJ at 150 °C which correspond to less than 3% of the total measured q_{obs} value during an experiment.

The experimental enthalpy of solution ($\Delta_{sol}H^{exp}$ in kJ/mol) is retrieved from q_{sol} and the total moles of dissolved solid (n_s) according to,

$$\Delta_{sol}H^{exp} = q_{sol} / n_s \quad (4)$$

The standard molal enthalpy of solution ($\Delta_{sol}H°$) is then obtained at a given temperature by linear regression of the experimental $\Delta_{sol}H^{exp}$ values measured in solutions with variable initial ionic strength and by extrapolation to infinite dilution. Test experiments indicate that for the dissolution of Nd hydroxide in perchloric acid based solutions with an ionic strength of 0.01 mol/kg it can be assumed that within experimental uncertainty $\Delta_{sol}H^{exp} = \Delta_{sol}H°$ (section 3.3).

2.4.2. Speciation calculation

The stability of Nd aqueous species and the solubility of Nd hydroxide were calculated in the experimental solutions using the GEMS code package v. 3.9.5 (Kulik et al., 2013), the TSolMod library for equations of state and activity model calculations (Wagner et al., 2012), and the MINES thermodynamic database (Gysi et al., 2023). Thermodynamic data used include the properties of aqueous species, gases, and solids in the Nd-Na-Cl-O-H component system. Aqueous species include Nd hydroxyl complexes (Haas et al., 1995), the Nd^{3+} aqua ion (Shock and Helgeson, 1988; Shock et al., 1997), Na-bearing aqueous species (Miron et al., 2016) and other aqueous species (Shock and Helgeson, 1988; Shock et al., 1997; Sverjensky et al., 1997). The dataset for Nd species was taken from the slop98.dat database originally

compiled for the SUPCRT92 program (Johnson et al., 1992), referred hereafter as "Supcrt92". The properties of the solids used include $Nd(OH)_3$(s) (Diakonov et al., 1998b; Navrotsky et al., 2015), NaCl(s) (Robie and Hemingway, 1995), and Nd_2O_3(s) (Konings et al., 2014; Navrotsky et al., 2015).

Thermodynamic properties for aqueous species are calculated at temperature and pressure of interest using the revised HKF equation-of-state (Helgeson et al., 1981; Tanger and Helgeson, 1988; Shock and Helgeson, 1988; Shock et al., 1992). The Peng-Robinson-Stryjek-Vera (PRSV) equation of state is used for gases (Stryjek and Vera, 1986; Proust and Vera, 1989). The properties of H_2O are calculated from the IAPS-84 equation-of-state (Kestin et al., 1984; Haar et al, 1984)

The activities of aqueous species were calculated at the experimental conditions using the initial pH of 2 in the perchloric acid based experimental starting solutions and the final measured Nd concentrations in the quenched experimental solutions. The activity coefficients (γ_i) of charged aqueous species were calculated using the extended Debye-Hückel equation (Robinson and Stokes, 2002),

$$log\gamma_i = \frac{-Az_i^2\sqrt{I}}{1+\mathring{a}B\sqrt{I}} + \Gamma_\gamma + b_\gamma I \quad (5)$$

where A and B are the temperature and pressure dependent Debye-Hückel parameters (Helgeson et al., 1981; Wagner et al., 2014); b_γ is the extended term parameter, $\mathring{a}$ is the ion size parameter assumed to be a common value for given background electrolyte model (Helgeson et al., 1981); Γ_γ is a mole fraction to molality conversion factor. The value b_γ varies between

0.21 to 0.24 from 150 to 25 °C in perchlorate ($NaClO_4/HClO_4$) aqueous solutions as determined based on hydrothermal REE speciation experiments (Migdisov and Williams-Jones, 2007). The value *I* is the effective ionic strength calculated from,

$$I = \frac{1}{2}\sum_i m_i z_i^2 \quad (6)$$

where m_i is the molal concentration and z_i is the charge of the species in the solution. The activity coefficients of neutral species are assumed to be equal to unity.

3. RESULTS

3.1. Characterization of crystalline $Nd(OH)_3$(s)

X-ray diffraction analysis of the $Nd(OH)_3$(s) powders synthesized hydrothermally indicates the formation of pure crystalline solids (Fig. 2). Comparison to two available XRD reference patterns by Beall et al. (1976) and Roy and McKinstry (1953) shows a perfect peak match to the hexagonal ($P6_3/m$) crystal structure of Nd hydroxide, with major reflections at Miller indices of (100), (110) and (101). The XRD spectra display sharp peaks and low background signals. The refined unit cell parameters are close to those refined in previous studies (Table 1).

Raman spectroscopy using the 532 nm excitation laser was conducted to verify any possible contamination of the synthesized $Nd(OH)_3$ solids by the presence of trace CO_2 (Diakonov et al., 1998b). Lattice vibrational and REE-O stretching modes of $Nd(OH)_3$(s) are present in the spectral region of 40−800 cm^{-1}; the OH vibrational mode is found at ~3600 cm^{-1} similar to other measured REE hydroxides in the study by Hurtig et al (2024). A very small

peak is observed at 1073 cm^{-1}, which is consistent with the Raman modes of 1071 cm^{-1} for $La(OH)_3$ and of 1084 cm^{-1} for $Y(OH)_3$ (Hurtig et al, 2024). No major C-O symmetric stretching bands (visible for calcite between 1000 and 1200 cm^{-1}) are observed in our analysis, indicating that the solids synthesized are pure and carbonate-free. Figure 3 shows a comparison between the spectra of $Nd(OH)_3$(s) and reference spectra for both calcite and bastnäsite-(Ce).

3.2. Validation experiments for the enthalpy of solution of NaCl(s)

Validation experiments were conducted to assess the accuracy of the calorimetric method developed in this study. These validation experiments were carried out by dissolving varying amounts of NaCl(s) at 148.5 ±0.05 °C to measure the enthalpy of solution at an ionic strength ranging between 0.05 to 0.24 mol/kg NaCl. Figure 4a shows the heat flow signals as a function of time with an exothermic peak becoming larger with increased ionic strength due to the increased total amount of dissolved NaCl. Integration of each of the heat flow curves over a duration of 1 h is used to retrieve the $\Delta_{sol}H^{exp}$ values for NaCl according to Eqs. 2-4 with the results listed in Table 2.

The measured $\Delta_{sol}H^{exp}$ values for NaCl (i.e., for the reaction $NaCl(s) \rightarrow Na^+ + Cl^-$) as a function of ionic strength are shown in Figure 5a. Extrapolation of the measured $\Delta_{sol}H^{exp}$ values to infinite dilution employing the least squares method and a 95% confidence level yields a standard enthalpy of solution $\Delta_{sol}H°$ for NaCl(s) of -5.25 ± 0.25 kJ/mol (1σ). This experimental result is close to the predicted value of -5.42 kJ/mol at 148.5 °C. The latter is within the 95 % confidence bound of the fitted experimental data and was calculated using the properties of

NaCl(s) from Robie and Hemingway (1995), Na^+ from Miron et al. (2016), and Cl^- from Shock and Helgeson (1988), Cox et al. (1989), and Miron et al. (2016).

3.3. Enthalpy of solution of $Nd(OH)_3$(s)

3.3.1. Experimental enthalpy of solution of $Nd(OH)_3$(s) as a function of ionic strength and extrapolation to infinite dilution

Three sets of test experiments were carried out to determine the $\Delta_{sol}H^{exp}$ values for $Nd(OH)_3$(s) at an ionic strength of 0.01, 0.05, and 0.09 mol/kg $NaClO_4$ (Table 3). The measured heat flow curves for experiments conducted at 24.2 and 48.9 °C (Fig. 4) are characterized by an exothermic peak during the dissolution of $Nd(OH)_3$(s) (Eq. 1) which achieves a steady state after ~1 h. The exothermic heat flow curves vary little with ionic strength and are smaller than for the NaCl validation experiments due to the low solubility of $Nd(OH)_3$(s).

The experimental results indicate a slight increase in $\Delta_{sol}H^{exp}$ values with ionic strength (Fig. 5b,c). Experiments conducted at 24.2 °C and an ionic strength of 0.09 yield an average $\Delta_{sol}H^{exp}$ value of -143.4 ±2.7 kJ/mol and experiments performed at an ionic strength of 0.01 yield an average $\Delta_{sol}H^{exp}$ value of -146.2 ±0.5 kJ/mol. Experiments conducted at 48.9 °C and an ionic strength of 0.09 yields an average $\Delta_{sol}H^{exp}$ value of -145.0 ±3.3 kJ/mol and experiments performed at an ionic strength of 0.01 yield an average $\Delta_{sol}H^{exp}$ value of -148.7 ±1.6 kJ/mol.

Replicate experiments indicate a considerable decrease in uncertainty for experiments conducted at the lowest ionic strength (Fig. 5). Furthermore, extrapolation of the fitted experimental data to infinite dilution results in $\Delta_{sol}H°$ values that lie within the experimental

uncertainties of replicate experiments conducted at an ionic strength of 0.01. Consequently, the experimental $\Delta_{sol}H^{exp}$ values determined at the lowest ionic strength can be considered, within experimental uncertainty, to be equivalent to the $\Delta_{sol}H°$ values extrapolated to infinite dilution.

3.3.2. Standard molal enthalpy of solution of $Nd(OH)_3$(s) as a function of temperature and derivation of the heat capacity, entropy, and Gibbs energy of solution

The standard molal enthalpies of solution for $Nd(OH)_3$(s) were determined from 25 to 150 °C (Table 3, Fig. 6a). The experimental data display an overall decrease in $\Delta_{sol}H°$ values with increased temperature. The uncertainties based on replicate experiments range between 0.5 and 3.0 kJ/mol, representing an uncertainty better than 2 %. The measured enthalpy of solution ($\Delta_{sol}H°$) are fitted to an empirical equation (Haas and Fisher, 1976) to compute thermodynamic properties based on four parameters (h_{Tr}, a_0, a_1, and a_2; Table 4),

$$\Delta H°(T) = h_{Tr} + a_0\, T + (a_1 / 2)\, T^2 - a_2 / T \quad (7)$$

where h_{Tr} is a constant enthalpy term included according to,

$$h_{Tr} = \Delta H°(T_r) - a_0\, T_r - (a_1 / 2)\, T_r^2 + a_2/T_r \quad (8)$$

A series of fitting tests were performed to avoid over-parametrization of Eq. 7 and to derive an accurate heat capacity function (Supplementary Materials). The regressed coefficients of the fits (a_0-a_2) are listed in Table 4. Figure 6b shows the measured standard molal enthalpy increments of $Nd(OH)_3$(s) as a function of temperature, the regressed fits, and the 95 %

confidence bounds. Equations (7-8) are used to evaluate the heat capacity ($\Delta C_p°$) function from Kirchhoff's equation,

$$\Delta Cp^o = \frac{\partial \Delta H^o}{\partial T}_P \quad (9)$$

resulting in a Maier-Kelley heat capacity equation (Maier and Kelley, 1932) expressed as a function of T,

$$\Delta C_p° = a_0 + a_1 T + a_2 T^{-2} \quad (10)$$

The resulting fits and derived heat capacity of solution function with their corresponding 95 % confidence bounds are shown in Figure 6c. The behavior of the $\Delta C_p°$ function of aqueous species is influenced by the variation of the thermal expansion of water ($\partial\alpha/\partial T$) that exhibits a convex shape with an inflection point at 60−110°C (Anderson, 1991). This shape is in line with the derived heat capacity of solution function based on the fitted enthalpy values using a 4 parameters equation. This results in $\Delta_{sol}C_p$ values at 25 °C of -59 ±17 J/mol·K with an inflection point at ~75 °C, whereas other fits with less parameters result in a linear $\Delta_{sol}C_p$ function (Supplementary Materials).

The entropy of solution ($\Delta_{sol}S°$) is derived from the heat capacity function (Eq. 10) at temperature T according to the relation,

$$\Delta_{sol} S^o = \Delta_{sol} S^o_{Tr} + \int_{Tr}^{T} \frac{\Delta_{sol} Cp}{T} dT \quad (11)$$

resulting in the following integrated form,

$$\Delta_{sol}S^\circ = \Delta_{sol}S^\circ_{Tr} + a_0 \cdot \ln(T/T_r) + a_1 \cdot (T - T_r) + a_2/2\,(T^2 - T_r^2) \quad (12)$$

An $\Delta_{sol}S^\circ_{Tr}$ value of -127.19 ± 3.36 J/mol·K is obtained by combining the absolute entropy of the compounds involved in Eq. (1) and the properties listed in Tables 6 and 7. The latter include S°_{Nd3+} (-207.11 ±3.3 J/mol·K) from Morss (1976), $S^\circ_{H2O(aq)}$ (69.92 ±0.03 J/mol·K) from Cox et al. (1989), and $S^\circ_{Nd(OH)3(s)}$ (129.9 ±0.2 J/mol·K) from Chirico and Westrum (1980). The standard molal Gibbs energy of solution ($\Delta_{sol}G^\circ$) is retrieved at each temperature using the following relationship,

$$\Delta G^\circ = \Delta H^\circ - T \cdot \Delta S^\circ \quad (13)$$

The smoothed fitted $\Delta_{sol}S^\circ$ and $\Delta_{sol}G^\circ$ values are listed in Table 5 together with their corresponding 95 % confidence bounds; their functions are shown in Figure 7.

DISCUSSION

4.1. Experimental versus predicted enthalpy of solution and discrepancies resulting from the thermodynamic properties of $Nd(OH)_3(s)$ and Nd^{3+}

The experimentally derived $\Delta_{sol}H^\circ$ values can be compared with the predicted values from tabulated thermodynamic data. The predicted $\Delta_{sol}H^\circ$ values are calculated from Δ_fH° values for $Nd(OH)_3(s)$ and the Nd^{3+} aqua ion (Tables 6 and 7) involved in Eq. 1 according to,

$$\Delta_{sol}H^\circ = \Delta_fH^\circ(Nd^{3+}) + 3\Delta_fH^\circ(H_2O(aq)) - \Delta_fH^\circ(Nd(OH)_3(s)) - 3\Delta_fH^\circ(H^+) \quad (14)$$

Aqueous speciation calculations indicate that $NdOH^{2+}$ is an additional aqueous species that could contribute to the measured $\Delta_{sol}H^\circ$ values at the experimental conditions (Fig. 8). The

corresponding enthalpy of solution involving this species can be described by,

$$\Delta_{sol}H° = \Delta_fH°(NdOH^{2+}) + 2\Delta_fH°(H_2O(aq)) - \Delta_fH°(Nd(OH)_3(s)) - 2H^+ \quad (15)$$

Figure 9a shows a comparison between the measured experimental $\Delta_{sol}H°$ values, the predicted $\Delta_{sol}H°$ values from thermodynamic tables, and the modeled $\Delta_{sol}H°$ values considering the proportions of each Nd species (i.e., Nd^{3+} and $NdOH^{2+}$ from Fig. 8). The predicted $\Delta_{sol}H°$ values to form Nd^{3+} are calculated using the properties of Nd^{3+} from Shock et al. (1997) and two different mineral properties for $Nd(OH)_3(s)$ compiled by Navrotsky et al. (2015). The predicted $\Delta_{sol}H°$ values to form $Nd(OH)^{2+}$ are calculated using the properties of Nd hydroxyl complexes derived by Haas et al (1995). Independent of the reliability of the thermodynamic properties for Nd hydroxyl complexes, the predicted $\Delta_{sol}H°$ values involving the $Nd(OH)^{2+}$ species should be larger in comparison to those involving the Nd^{3+} species because the two moles of $H_2O(aq)$ on the product side of Eq. 15. The measured $\Delta_{sol}H°$ values from our experiments are closer or lower than the $\Delta_{sol}H°$ values predicted from Eq. (14) involving only the Nd^{3+} species (Fig. 9a). In contrast, the modeled $\Delta_{sol}H°$ values considering the predicted stabilities of both $Nd^{3+}$and $NdOH^{2+}$ aqueous complexes display very large deviations from the experimental data and reach over 50 kJ/mol at 150 °C. Thus, the enthalpy measured in the experiments is controlled by the Nd^{3+} aqua ion (Eqs. 1 and 14) between 25 and 150 °C with negligible contribution from the $NdOH^{2+}$ species. Wood et al. (2002) observed a similar predominance of Nd^{3+} over $NdOH^{2+}$ based on potentiometric experiments carried out in acidic solutions up to 290 °C.

Further inspection of the thermodynamic properties of $Nd(OH)_3(s)$ compiled by

Navrotsky et al. (2015) and Diakonov et al. (1998b) indicate several sources of data for this solid (Table 7). A consistent set is provided for the heat capacity function from Chirico and Westrum (1980) and from Diakonov et al. (1998a, 1998b). In contrast, the enthalpy of formation of $Nd(OH)_3$(s) derived from previous experiments can vary highly with a $\Delta_f H°$ value of -1403.7 ±1.0 kJ/mol derived by Morss et al. (1989) and a value of -1415.6 ± 2.3 kJ/mol derived by Merli et al. (1997). The latter is the recommended value by Navrotsky et al. (2015) and also adopted in this study. A comparison of the $\Delta_{sol}H°$ curves predicted using these two sources of data (Fig. 9b) results in large deviations in comparison to the measured experimental values. The data from Merli et al. (1997) results in deviations of >5−7 kJ/mol and the data from Morss et al. (1989) in deviation <5 kJ/mol. These discrepancies indicate that the properties of Nd^{3+} from Supcrt92 (Table 6) need to be further evaluated because these trends cannot be explained solely by the uncertainty of the properties of $Nd(OH)_3$(s). The latter are in the order of ~1-2 kJ/mol based on calorimetric measurements (Table 7).

4.2. Derivation of the standard partial molal enthalpy and heat capacity function of Nd^{3+}

The standard partial molal enthalpy of formation ($\Delta_f H°$) of Nd^{3+} is retrieved as a function of temperature by solving Eq. 14 and using the properties of $Nd(OH)_3$(s) from Merli et al. (1997) combined with the experimental $\Delta_{sol}H°$ values and fits derived in this study (Tables 3 and 4). The $\Delta_f H°$ values for Nd^{3+} derived from the experimental enthalpy data were fit as a function of temperature using Eqs. (7-8) to retrieve the enthalpy increments and the heat capacity function according to Eq. (10). The resulting calculated values and fits are shown in Figure 10. The

436 regression coefficients a_0−a_2 are listed in Table 8 and the smoothed fitted $\Delta_f H°$ and $C_p°$ values
437 are listed in Table 9 together with their corresponding 95 % confidence bounds. The resulting
438 $\Delta_f H°$ value for Nd^{3+} at a reference condition of 25 °C and 1 bar is -704.4 ±0.5 kJ/mol.

439 Figure 11a-b shows a comparison between the experimentally derived $\Delta_f H°$ values for
440 Nd^{3+} and the predicted values as a function of temperature based on the thermodynamic
441 properties and HKF parameters tabulated in Shock et al. (1997) and references therein (i.e.,
442 Supcrt92, Table 6). The experimentally derived $\Delta_f H°$ values are systematically more negative
443 by ~7.5−8 kJ/mol in comparison to the predictions calculated based on Shock et al. (1997).
444 The $C_p°$ function derived from our experimental data is however very close to the $C_p°$ values
445 from Supcrt92 (Fig. 11c-d). Therefore, the HKF parameters seem to reproduce the overall
446 temperature function (i.e., heat capacity and entropy) derived for the Nd^{3+} aqua ion in the
447 studied temperature range. However, the ~7.5−8 kJ/mol offset for the $\Delta_f H°$ values needs to be
448 corrected, and hence requires an adjustment of the standard partial molal Gibbs energy $\Delta_f G°$
449 value at 25 °C and 1 bar (Eq. 13).

450 Different studies retrieved the $\Delta_f H°$ values for Nd^{3+} (Table 6) based on solution
451 calorimetric experiments for the reaction: $NdCl_3 \cdot nH_2O(s) \rightleftharpoons Nd^{3+} + 3Cl^- + n \cdot H_2O(aq)$.
452 Cordfunke and Konings (2001b) evaluated those literature data and reported a $\Delta_f H°$ value for
453 Nd^{3+} of -694.8 ±2.0 kJ/mol. However, this value relies on the $\Delta_f H°$ value for $NdCl_3(s)$ which
454 shows a large scatter (~10-20 kJ/mol) in different studies (Table 7) due to the hydrated nature
455 of this solid. Therefore, the observed discrepancies between measured and calculated $\Delta_f H°$
456 values for Nd^{3+} (Fig. 11a-b) are quite plausible and likely associated with its derivation in
457 Supcrt92 from the properties of the Nd chloride solid (Table 6; Spedding and Miller, 1952 and

458 Morss, 1976).

459

460 **4.3. Derivation of the standard molal Gibbs energy of formation of Nd^{3+} as a function of**
461 **temperature and comparison to previous studies**

462 The standard molal Gibbs energy of formation ($\Delta_f G°$) of the Nd^{3+} aqua ion is calculated from
463 the standard Gibbs energy of solution $\Delta_{sol} G°$ (Eq. 1) according to,

464 $$\Delta_f G°(Nd^{3+}) = \Delta_{sol} G° - 3 \cdot \Delta_f G°[H_2O(aq)] + \Delta_f G°[Nd(OH)_3(s)] \quad (16)$$

465 The smoothed $\Delta_{sol} G°$ values are obtained at each temperature from the fitted $\Delta_{sol} H°$ and $\Delta_{sol} S°$
466 values according to Eq. (13). The resulting $\Delta_f G°(Nd^{3+})$ function (Tables 8 and 9) derived from
467 our experimental data is compared to the predicted values from Supcrt92 in Figure 11e-f. This
468 comparison indicates an almost constant discrepancy between 25 and 150 °C but the overall
469 function reproduces the increase in $\Delta_f G°$ values with temperature observed in our experiments.
470 Hence, a correction is necessary for the $\Delta_f G°(Nd^{3+})$ value at reference conditions of 25 °C and
471 1 bar. The recommended $\Delta_f G°(Nd^{3+})$ value derived in this study is -679.7 ±0.7 kJ/mol and can
472 either be used with the HKF parameters from Table 6 or the empirically derived heat capacity
473 function from Tables 8 and 9. The resulting updated speciation model for Nd^{3+} and Nd
474 hydroxyl aqueous species (Fig. 12) indicates the predominance of Nd^{3+} over $Nd(OH)^{2+}$ in the
475 temperature range of 25 – 150 °C. The increased stability of $Nd(OH)^{2+}$ with temperature is still
476 uncertain because its thermodynamic properties are still based on the hydrolysis constant from
477 Haas et al. (1995), which likely needs to be revised or verified.

478 A recent thermodynamic optimization study by Pan et al. (2024) indicates a need to

reassess the properties of the REE^{3+} aqua ions in order to accurately model the solubility of REE phosphates. The optimized $\Delta_f G°$ value for Nd^{3+} tabulated in Pan et al. (2024) is -681.7 ±1 kJ/mol which is very close to the value derived in our study (Table 6). The experimental solubility data assessed by Pan et al. (2024) include a broad dataset for monazite, rhabdophane, and xenotime between 25 and 300 °C, giving confidence that the $\Delta_f G°$ value for Nd^{3+} retrieved in our study is accurate.

The formation constants for the Nd chloride and fluoride aqueous species were derived in the hydrothermal solubility experiments by Migdisov et al. (2009) at temperatures up to 300 °C according to the following reactions,

$$Nd^{3+} + Cl^- \rightleftharpoons NdCl^{2+} \ (\log\beta_{Cl}{}^1) \quad (17)$$

$$Nd^{3+} + 2Cl^- \rightleftharpoons NdCl_2{}^+ \ (\log\beta_{Cl}{}^2) \quad (18)$$

$$Nd^{3+} + F^- \rightleftharpoons NdF^{2+} \ (\log\beta_F{}^1) \quad (19)$$

In order to keep internal consistency with the properties of Nd^{3+} derived in our study, the $\Delta_f G°$ have to be adjusted by -8.1 kJ/mol for all of the Nd chloride and fluoride species above. The updated recommended properties for $NdCl^{2+}$, $NdCl_2{}^+$ and NdF^{2+} are tabulated in Table 6 and can be used with the HKF parameters to correctly reproduce the $\log\beta$ from the solubility experiments by Migdisov et al. (2009).

4.4. Implications for modeling the solubility of monazite

Monazite is a common mineral found in REE mineral deposits associated to alteration zones

and hydrothermal veins (Smith et al., 2000, 2016; Harlov et al., 2016). Aqueous fluids play an important role in the mobility of REE in these deposits, which is controlled by the formation of aqueous complexes and the solubility of the REE minerals. Hydrothermal $NdPO_4$ solubility experiments were carried out in a few previous studies (Poitrasson et al., 2004; Cetiner et al., 2005; Van Hoozen et al., 2020) from which solubility constants were retrieved between 25 and 250 °C. Thus, a comparison of the modeled monazite solubility with previously reported experiments can be used to assess the reliability of the retrieved thermodynamic properties in our study. The following reaction describes the $NdPO_4$ solubility product,

$$NdPO_4(s) \rightleftharpoons Nd^{3+} + PO_4^{3-} \ (K_{s0}) \quad (20)$$

which is retrieved from the thermodynamic properties listed in Tables 6 and 7. Conversion to equilibrium the constant is done according to,

$$\Delta_r G^\circ = \Delta_f G^\circ [Nd^{3+}] + \Delta_f G^\circ [PO_4^{3-}] - \Delta_f G^\circ [NdPO_4(s)] \quad (21)$$

$$\log K_{s0} = -\Delta_r G^\circ / RT\ln(10) \quad (22)$$

where R is the ideal gas constant and T is the temperature in K.

The calculated solubility products based on the optimized properties of the Nd^{3+} aqua ion derived in this study display an excellent agreement with the experimental data between 100 and 300 °C (Fig. 13). The latter are from the studies by Van Hoozen et al. (2020), Poitrasson et al. (2004) and Cetiner et al. (2005). The calculated $\log K_{s0}$ values predicted using the Nd^{3+} aqua ion from Supcrt92 are systematically smaller by ~0.5-1.5 orders of magnitude. This comparison gives confidence that the adjusted $\Delta_r G^\circ$ values recommended in Table 6 together with the properties of the HKF parameters from Table 6 or the empirical heat capacity

function from Table 8 can be used to accurately predict the thermodynamic properties of the Nd^{3+} aqua ion between 25 and 300 °C.

5. CONCLUSIONS

Hydrothermal solution calorimetric experiments were used to measure the enthalpy of solution of $Nd(OH)_3$(s) and retrieve the enthalpy of formation of the Nd^{3+} aqua ion at temperatures ranging from 25 to 150 °C. The recommended thermodynamic properties to accurately assess the stability of the Nd^{3+} aqua ion are listed in Table 6.

The standard partial molal enthalpy of formation $\Delta_f H°$ of Nd^{3+} derived from the experimental study displays differences of up to 10 kJ/mol compared to the enthalpy values derived from the HKF equation of state in the studied temperature range. These discrepancies are caused due to previously reported $\Delta_f H°$ values for Nd^{3+} (Speeding and Miller, 1952) at reference state (25 °C and 1 bar). Nevertheless, these inaccuracies are resolved by adjusting the standard partial molal Gibbs energy of formation $\Delta_f G°$ of Nd^{3+} at 25 °C and 1 bar from -672.0 (Supcrt92) to -679.7 kJ/mol (this study). Similar adjustments were proposed by Pan et al. (2024) for modeling the solubility of all of the REE phosphate endmembers (i.e. for both monazite and xenotime) to 300 °C. The heat capacity, enthalpy, and entropy temperature dependent empirical equation derived from our calorimetric study are also provided (Table 8, Eqs. 7-10), and a comparison to previous monazite-(Nd) solubility experiments, indicates that these functions can at least be extrapolated to 300 °C.

The results from this study indicate that the thermodynamic properties for the REE^{3+}

aqua ions reported at reference conditions and compiled in Sucprt92 (Shock and Helgeson, 1988; Shock et al., 1997) need to be further scrutinized because the adjustments required for other REE are currently unknown. Nevertheless, the thermodynamic optimization study by Pan et al. (2024) provides an internally consistent updated dataset for the REE^{3+} aqua ion that agrees with the experimental results presented here. Furthermore, calorimetric experiments provide further confidence that the HKF parameters might reproduce the temperature functions accurately at least in subcritical aqueous fluids. Hence, an adjustment of the $\Delta_f G°$ values at 25 °C and 1 bar might be a reasonable approach to model the stability of each aqua ions. As demonstrated in this study, such adjustments have important implications to accurately model the stability of monazite in hydrothermal aqueous fluids. This study contributes to the development of MINES thermodynamic database (Gysi et al., 2023), which is an internally consistent thermodynamic dataset for modeling the behavior of REE in hydrothermal systems.

CREDIT AUTHORSHIP CONTRIBUTION STATEMENT

Yerko Figueroa Penarrieta: Data curation, Methodology, Investigation, Writing – original draft, Writing – review & editing. **Alexander P. Gysi**: Conceptualization, Funding acquisition, Methodology, Investigation, Project administration, Supervision, Writing – review & editing.

DECLARATION OF COMPETING INTEREST

The authors declare that they have no known competing financial interests or personal relationships that could have appeared to influence the work reported in this paper.

DATA AVAILABILITY

Data are available through Mendeley Data at https://doi.org/10.17632/6s6zzsbjxb.1

ACKNOWLEDGMENTS

This research is based upon work supported by the U.S. Department of Energy, Office of Science, Office of Basic Energy Sciences, Geosciences program under Award Number DE-SC0021106 to AG. Raman analyses at the New Mexico Bureau of Geology and Mineral Resources were supported through a EAR-2117061 major research instrumentation grant from the National Science Foundation. We would like to thank Dr. N. Hurtig and Dr. S. Smith for their help for the Raman analysis, and Dr. H. Han and B. Frey for their support on the ICP-OES instrument. We appreciate the detailed comments and suggestion of three anonymous reviewers that contributed to the quality of the article. We also want to thank Executive Editor Jeffrey Catalano for handling this manuscript.

APPENDIX A. Supplementary Material

The Supplementary Material includes Figure S1 with different fits to Eqs. 7-10.

REFERENCES

Anderson G. M., Castet S., Schott J. and Mesmer R. E. (1991) The density model for estimation of thermodynamic parameters of reactions at high temperatures and pressures. *Geochim. Cosmochim. Acta* **55,** 1769–1779.

Arcis H., Coulier Y., Ballerat-Busserolles K., Rodier L. and Coxam J.-Y. (2014) Enthalpy of solution of CO_2 in aqueous solutions of primary alkanolamines: A comparative study of hindered and nonhindered amine-based solvents. *Ind. Eng. Chem. Res.* **53**, 10876–

10885.

Baes J. and Mesmer R. E. (1981) Thermodynamics of cation hydrolysis. *Am. J. Sci.* **281**, 935–962.

Beall G. W., Milligan W. O., Dillin D. R., Williams R. J. and McCoy J. J. (1976) Refinement of neodymium trihydroxide. *Acta Cryst. B* **32**, 2227–2229.

Beland C. M. J. and Williams-Jones A. E. (2021) The genesis of the Ashram REE deposit, Quebec: Insights from bulk-rock geochemistry, apatite-monazite-bastnäsite replacement reactions and mineral chemistry. *Chem. Geol.* **578**, 120298.

Belsky A., Hellenbrandt M., Karen V. L. and Luksch P. (2002) New developments in the Inorganic Crystal Structure Database (ICSD): accessibility in support of materials research and design. *Acta Cryst. B* **58**, 364–369.

Calvet E. and Prat H. (1963) *Recent Progress in Microcalorimetry*., Pergamon Press, New York.

Cetiner Z. S., Wood S. A. and Gammons C. H. (2005) The aqueous geochemistry of the rare earth elements. Part XIV. The solubility of rare earth element phosphates from 23 to 150 °C. *Chem. Geol.* **217**, 147–169.

Chirico R. D. and Westrum E. F. (1980) Thermophysics of the lanthanide trihydroxides II. Heat capacities from 10 to 350 K of $Nd(OH)_3$ and $Tb(OH)_3$. Lattice and Schottky contributions. *J. Chem. Thermodyn.* **12**, 311–327.

Cordfunke E. H. P., Booij A. S. and Furkaliouk M. Yu. (1996) The standard molar enthalpies of formation of the rare earth trihalides IV. $DyCl_3$(s) and $NdCl_3$(s). *J. Chem. Thermodyn.* **28**, 1387–1393.

Cordfunke E. H. P and Konings R. J. M. (2001a) The enthalpies of formation of lanthanide compounds: I. $LnCl_3$(cr), $LnBr_3$(cr) and LnI_3(cr). *Thermochim. Acta* **375**, 17–50.

Cordfunke E. H. P and Konings R. J. M. (2001b) The enthalpies of formation of lanthanide compounds: II. Ln^{3+}(aq). *Thermochim. Acta* **375**, 51–64.

Cordfunke E. H. P. and Konings R. J. M. (2001c) The enthalpies of formation of lanthanide compounds: III. Ln_2O_3(cr). *Thermochim. Acta* **375**, 65–79.

Coulier Y. and Tremaine P. R. (2014) Standard partial molar heat capacities and enthalpies of formation of aqueous aluminate under hydrothermal conditions from integral heat of solution measurements. *J. Chem. Thermodyn.* **78**, 79–92.

Cox J. D., Wagman D. D. and Medvedev V. A. (1989) *CODATA key values for*

thermodynamics., Hemisphere Pub. Corp., New York.

Diakonov I. I, Ragnarsdottir K. V. and Tagirov B. R. (1998a) Standard thermodynamic properties and heat capacity equations of rare earth hydroxides:: II. Ce(III)-, Pr-, Sm-, Eu(III)-, Gd-, Tb-, Dy-, Ho-, Er-, Tm-, Yb-, and Y-hydroxides. Comparison of thermochemical and solubility data. *Chem. Geol.* **151**, 327–347.

Diakonov I. I., Tagirov B. R. and Ragnarsdottir K. V. (1998b) Standard thermodynamic properties and heat capacity equations for rare earth element hydroxides: I . $La(OH)_3$(s) and $Nd(OH)_3$(s). Comparison of thermochemical and solubility data. *Radiochim. Acta* **81**, 107–116.

Djamali E. and Cobble J. W. (2009) Standard state thermodynamic properties of aqueous sodium chloride using high dilution calorimetry at extreme temperatures and pressures. *J. Phys. Chem. B* **113**, 5200–5207.

Dushyantha N., Batapola N., Ilankoon I. M. S. K., Rohitha S., Premasiri R., Abeysinghe B., Ratnayake N. and Dissanayake K. (2020) The story of rare earth elements (REEs): Occurrences, global distribution, genesis, geology, mineralogy and global production. *Ore Geol. Rev.* **122**, 103521.

Fitzgibbon G. C., Holley Jr C. E. and Wadsö I. (1965) The Heat of Formation of Lanthanum Oxide1. *J. Phys. Chem.* **69**, 2464–2466.

Gysi A. P. and Harlov D. (2021) Hydrothermal solubility of $TbPO_4$, $HoPO_4$, $TmPO_4$, and $LuPO_4$ xenotime endmembers at pH of 2 and temperatures between 100 and 250 °C. *Chem. Geol.* **567**, 120072.

Gysi A. P., Harlov D. and Miron G. D. (2018) The solubility of monazite ($CePO_4$), $SmPO_4$, and $GdPO_4$ in aqueous solutions from 100 to 250 °C. *Geochim. Cosmochim. Acta* **242**, 143–164.

Gysi A. P., Hurtig, N.C., Pan, R., Miron, G.D., and Kulik, D.A. (2023) MINES thermodynamic database, New Mexico Bureau of Geology and Mineral Resources, version 23. https://doi.org/10.58799/mines-tdb

Gysi A. P. and Williams-Jones A. E. (2013) Hydrothermal mobilization of pegmatite-hosted REE and Zr at Strange Lake, Canada: A reaction path model. *Geochim. Cosmochim. Acta* **122**, 324–352.

Gysi A. P., Williams-Jones A. E. and Collins P. (2016) Lithogeochemical Vectors for Hydrothermal Processes in the Strange Lake Peralkaline Granitic REE-Zr-Nb Deposit. *Econ. Geol.* **111**, 1241–1276.

Gysi A. P., Williams-Jones A. E. and Harlov D. (2015) The solubility of xenotime-(Y) and

other HREE phosphates ($DyPO_4$, $ErPO_4$ and $YbPO_4$) in aqueous solutions from 100 to 250 °C and p_{sat}. *Chem. Geol.* **401**, 83–95.

Haar L., Gallagher J. S. and Kell G. S. (1984) *NBS/NRC steam tables thermodynamic and transport properties and computer programs for vapor and liquid states of water in SI units.* Hemisphere pub., Washington, D. C.

Haas J. R., Shock E. L. and Sassani D. C. (1995) Rare earth elements in hydrothermal systems: Estimates of standard partial molal thermodynamic properties of aqueous complexes of the rare earth elements at high pressures and temperatures. *Geochim. Cosmochim. Acta* **59**, 4329–4350.

Hakin A. W., Lukacs M. J., Liu J. L., Erickson K. and Madhavji A. (2003) The volumetric and thermochemical properties of $Y(ClO_4)_3$(aq), $Yb(ClO_4)_3$(aq), $Dy(ClO_4)_3$(aq), and $Sm(ClO_4)_3$(aq) at T = (288.15, 298.15, 313.15, and 328.15) K and p = 0.1 MPa. *J. Chem. Thermodyn.* **35**, 775–802.

Harlov D. E., Meighan C. J., Kerr I. D. and Samson I. M. (2016) Mineralogy, chemistry, and fluid-aided evolution of the Pea Ridge Fe oxide-(Y+REE) deposit, Southeast Missouri, USA. *Econ. Geol.* **11**, 1963–1984.

Helgeson H. C., Kirkham D. H. and Flowers G. C. (1981) Theoretical prediction of the thermodynamic behavior of aqueous electrolytes by high pressures and temperatures; IV, Calculation of activity coefficients, osmotic coefficients, and apparent molal and standard and relative partial molal properties to 600 °C and 5kb. *Am. J. Sci.* **281**, 1249–1516.

Huber E. J. and Holley Jr C. E. (1952) The heat of combustion of Neodymium. *J. Am. Chem. Soc.* **74**, 5530–5531.

Hurtig N. C., Gysi A. P., Smith-Schmitz S. E. and Harlov D. (2024) Raman spectroscopic study of anhydrous and hydrous REE phosphates, oxides, and hydroxides. *Dalton Trans.* **53**, 9964–9978.

Johnson J. W., Oelkers E. H. and Helgeson H. C. (1992) SUPCRT92: A software package for calculating the standard molal thermodynamic properties of minerals, gases, aqueous species, and reactions from 1 to 5000 bar and 0 to 1000°C. *Comput. and Geosci.* **18**, 899–947.

Kestin J., Sengers J. V., Kamgar-Parsi B. and Sengers J. M. H. L. (1984) Thermophysical Properties of Fluid H_2O. *J. Phys. Chem. Ref. Data* **13**, 175–183.

Konings R. J. M., Beneš O., Kovács A., Manara D., Sedmidubský D., Gorokhov L., Iorish V. S., Yungman V., Shenyavskaya E. and Osina E. (2014) The Thermodynamic properties of the f-elements and their compounds. Part 2. The Lanthanide and Actinide oxides. *J.*

Phys. Chem. Ref. Data **43**, 013101.

Kulik D. A., Wagner T., Dmytrieva S. V., Kosakowski G., Hingerl F. F., Chudnenko K. V. and Berner U. R. (2013) GEM-Selektor geochemical modeling package: revised algorithm and GEMS3K numerical kernel for coupled simulation codes. *Comput. Geosci.* **17**, 1–24.

Lee J. H. and Byrne R. H. (1992) Examination of comparative rare earth element complexation behavior using linear free-energy relationships. *Geochim. Cosmochim. Acta* **56**, 1127–1137.

Long K. R., Van Gosen B. S., Foley N. K. and Cordier D. (2012) The Principal rare earth elements deposits of the United States: A summary of domestic deposits and a global perspective. In *Non-Renewable Resource Issues: Geoscientific and Societal Challenges* (eds. R. Sinding-Larsen and F.-W. Wellmer). International Year of Planet Earth. Springer Netherlands, Dordrecht. pp. 131–155.

Louvel M., Etschmann B., Guan Q., Testemale D. and Brugger J. (2022) Carbonate complexation enhances hydrothermal transport of rare earth elements in alkaline fluids. *Nat. Commun.* **13**, 1456.

Lutterotti L. (2000) Maud: a Rietveld analysis program designed for the internet and experiment integration. *Acta Crystallogr. A* **56**, 54.

Maier C. G. and Kelley K. (1932) An equation for the representation of high-temperature heat content data1. *J. Am. Chem. Soc.* **54**, 3243–3246.

Merli L., Lambert B. and Fuger J. (1997) Thermochemistry of lanthanum, neodymium, samarium and americium trihydroxides and their relation to the corresponding hydroxycarbonates. *J. Nucl. Mater.* **247**, 172–176.

Merli L., Rorif F. and Fuger J. (1998) The enthalpies of solution of lanthanide metals in hydrochloric acid at various concentrations. Relevance to nuclear waste long term storage. *Radiochim. Acta* **82**, 3–10.

Migdisov A. A. and Williams-Jones A. E. (2007) An experimental study of the solubility and speciation of neodymium (III) fluoride in F-bearing aqueous solutions. *Geochim. Cosmochim. Acta* **71**, 3056–3069.

Migdisov Art. A., Williams-Jones A. E. and Wagner T. (2009) An experimental study of the solubility and speciation of the Rare Earth Elements (III) in fluoride- and chloride-bearing aqueous solutions at temperatures up to 300°C. *Geochim. Cosmochim. Acta* **73**, 7087–7109.

Migdisov A. A. and Williams-Jones A. E. (2014) Hydrothermal transport and deposition of the

rare earth elements by fluorine-bearing aqueous liquids. *Miner Deposita* **49**, 987–997.

Migdisov A., Williams-Jones A. E., Brugger J. and Caporuscio F. A. (2016) Hydrothermal transport, deposition, and fractionation of the REE: Experimental data and thermodynamic calculations. *Chem. Geol.* **439**, 13–42.

Migdisov Art. A., Williams-Jones A. E. and Wagner T. (2009) An experimental study of the solubility and speciation of the Rare Earth Elements (III) in fluoride- and chloride-bearing aqueous solutions at temperatures up to 300°C. *Geochim. Cosmochim. Acta* **73**, 7087–7109.

Miron G. D., Wagner T., Kulik D. A. and Heinrich C. A. (2016) Internally consistent thermodynamic data for aqueous species in the system Na–K–Al–Si–O–H–Cl. *Geochim. Cosmochim. Acta* **187**, 41–78.

Morss L. R. (1976) Thermochemical properties of yttrium, lanthanum, and the lanthanide elements and ions. *Chem. Rev.* **76**, 827–841.

Morss L. R., Haar C. M. and Mroczkowski S. (1989) Standard molar enthalpy of formation of neodymium hydroxide. *J. Chem. Thermodyn.* **21**, 1079–1083.

Navrotsky A., Lee W., Mielewczyk-Gryn A., Ushakov S. V., Anderko A., Wu H. and Riman R. E. (2015) Thermodynamics of solid phases containing rare earth oxides. *J. Chem. Thermodyn.* **88**, 126–141.

Nisbet H., Migdisov A. A., Goncharov V., van Hinsberg V., Williams-Jones A. E., Xu H. and Guo X. (2022) The solubility and speciation of Nd in carbonate-bearing hydrothermal fluids up to 250 °C. *Chem. Geol.* **611**, 121122.

Pan R., Gysi A. P., Miron G. D. and Zhu C. (2024) Optimized thermodynamic properties of REE aqueous species (REE^{3+} and $REEOH^{2+}$) and experimental database for modeling the solubility of REE phosphate minerals (monazite, xenotime, and rhabdophane) from 25 to 300 °C. *Chem. Geol.* **643**, 121817.

Poitrasson F., Chenery S. and Bland D. J. (1996) Contrasted monazite hydrothermal alteration mechanisms and their geochemical implications. *Earth Planet. Sci. Lett.* **145**, 79–96.

Popa K., Jutier F., Wastin F. and Konings R. J. M. (2006) The heat capacity of NdPO4. *J. Chem. Thermodyn.* **38**, 1306–1311.

Pourtier E., Devidal J.-L. and Gibert F. (2010) Solubility measurements of synthetic neodymium monazite as a function of temperature at 2kbars, and aqueous neodymium speciation in equilibrium with monazite. *Geochim. Cosmochim. Acta* **74**, 1872–1891.

Proust P. and Vera J. H. (1989) PRSV: The stryjek-vera modification of the peng-robinson

equation of state. Parameters for other pure compounds of industrial interest. *Can. J. Chem. Eng.* **67**, 170–173.

Robie R. A. and Hemingway B. S. (1995) *Thermodynamic properties of minerals and related substances at 298.15 K and 1 bar (10^5 Pascals) pressure and at higher temperatures*., U.S. Geol. Surv. Bull. 2131.

Robinson R. A. and Stokes R. H. (2002) *Electrolyte Solutions: Second Revised Edition*., Courier Corporation, London.

Roy R. and McKinstry H. A. (1953) Concerning the so-called $Y(OH)_3$-type structure and the structure of La(OH)3. *Acta Cryst* **6**, 365–366.

Shock E. L. and Helgeson H. C. (1988) Calculation of the thermodynamic and transport properties of aqueous species at high pressures and temperatures: Correlation algorithms for ionic species and equation of state predictions to 5 kb and 1000°C. *Geochim. Cosmochim. Acta* **52**, 2009–2036.

Shock E. L., Oelkers E. H., Johnson J. W., Sverjensky D. A. and Helgeson H. C. (1992) Calculation of the thermodynamic properties of aqueous species at high pressures and temperatures. Effective electrostatic radii, dissociation constants and standard partial molal properties to 1000 °C and 5 kbar. *J. Chem. Soc., Faraday Trans.* **88**, 803–826.

Shock E. L., Sassani D. C., Willis M. and Sverjensky D. A. (1997) Inorganic species in geologic fluids: Correlations among standard molal thermodynamic properties of aqueous ions and hydroxide complexes. *Geochim. Cosmochim. Acta* **61**, 907–950.

Smith M. P., Henderson P. and Campbell L. S. (2000) Fractionation of the REE during hydrothermal processes: constraints from the Bayan Obo Fe-REE-Nb deposit, Inner Mongolia, China. *Geochim. Cosmochim. Acta* **64**, 3141–3160.

Smith M. P., Moore K., Kavecsánszki D., Finch A. A., Kynicky J. and Wall F. (2016) From mantle to critical zone: A review of large and giant sized deposits of the rare earth elements. *Geosci. Front.* **7**, 315–334.

Spedding F. H., Baker J. L. and Walters J. P. (1979) Apparent and partial molal heat capacities of aqueous rare earth nitrate solutions at 25. degree. C. *J. Chem. Eng. Data* **24**, 298–305.

Spedding F. H. and Miller C. F. (1952) Thermochemistry of the rare earths. I. Cerium and neodymium. *J. Am. Chem. Soc.* **74**, 4195–4198.

Stryjek R. and Vera J. H. (1986) PRSV: An improved peng—Robinson equation of state for pure compounds and mixtures. *Can. J. Chem. Eng.* **64**, 323–333.

Stuve J. M. (1965) Technical report USBM-RI-6697. *US Bureau of Mines*.

Sverjensky D. A., Shock E. L. and Helgeson H. C. (1997) Prediction of the thermodynamic properties of aqueous metal complexes to 1000°C and 5 kb. *Geochim. Cosmochim. Acta* **61**, 1359–1412.

Tanger J. C. and Helgeson H. C. (1988) Calculation of the thermodynamic and transport properties of aqueous species at high pressures and temperatures; revised equations of state for the standard partial molal properties of ions and electrolytes. *Am. J. Sci.* **288**, 19–98.

Ushakov S. V., Helean K. B., Navrotsky A. and Boatner L. A. (2001) Thermochemistry of rare-earth orthophosphates. *J. Mater. Res.* **16**, 2623–2633.

Van Hoozen C. J., Gysi A. P. and Harlov D. E. (2020) The solubility of monazite ($LaPO_4$, PrPO4, $NdPO_4$, and $EuPO_4$) endmembers in aqueous solutions from 100 to 250 °C. *Geochim. Cosmochim. Acta* **280**, 302–316.

Virtanen P., Gommers R., Oliphant T. E., Haberland M., Reddy T., Cournapeau D., Burovski E., Peterson P., Weckesser W. and Bright J. (2020) SciPy 1.0: fundamental algorithms for scientific computing in Python. *Nat. Methods* **17**, 261–272.

Wagner T., Kulik D. A., Hingerl F. F. and Dmytrieva S. V. (2012) GEM-Selektor geochemical modeling package: Tsolmod library and data interface for multicomponent phase models. *Can. Mineral.* **50**, 1173–1195.

Williams-Jones A. E., Migdisov A. A. and Samson I. M. (2012) Hydrothermal Mobilisation of the Rare Earth Elements – a Tale of "Ceria" and "Yttria." *Elements* **8**, 355–360.

Williams-Jones A. E., Samson I. M. and Olivo G. R. (2000) The Genesis of hydrothermal fluorite-REE deposits in the Gallinas Mountains, New Mexico. *Econ. Geol.* **95**, 327–341.

Wood A., Palmer D. A., Wesolowski D. J. and Benezeth P. (2002) The aqueous geochemistry of the rare earth elements and yttrium. Part XI. The solubility of $Nd(OH)_3$ and hydrolysis of Nd^{3+} from 30 to 290°C at saturated water vapor pressure with in-situ pHm measurement. *Geochem. Soc. Spec. Publ. No.7,* **7**, 229–256.

TABLES

Table 1. Refined unit cell parameters in the hexagonal structure ($P6_3/m$) for $Nd(OH)_3$(s) synthesized in this study and comparison those retrieved by Beall et al. (1976) from the COD database 210682 and Roy and McKinstry (1953).

Reference	Lattice parameters		
	a [Å]	c [Å]	Volume [Å^3]
This study	6.429 ±0.001	3.742 ±0.001	133.93
Beall et al. (1976)	6.422	3.742	133.65
Roy and McKinstry (1953)	6.421	3.74	133.5

Table 2. Results from the NaCl solution calorimetric experiments at 148.5 °C listing the measured integral heat of solution (q_{sol}) , blank corrections (q_{blk}), and derived experimental molal enthalpies ($\Delta_{sol}H^{exp}$) according to Eqs. (2-4).

$n_{NaCl(s)}$ (mol)	I (mol/kg)	q_{obs} (mJ)	q_{blk} (mJ)	q_{sol} (mJ)	$\Delta_{sol}H^{exp}$ (kJ/mol)
0.16	0.05	-778	-34.4	-743.1	-4.64
0.31	0.1	-1414	-34.3	-1380	-4.42
0.33	0.11	-1556	-34.8	-1521	-4.67
0.62	0.21	-2568	-34.3	-2534	-4.09
0.68	0.23	-2847	-34.6	-2813	-4.12
0.71	0.24	-2487	-34.3	-2452	-3.44

Table 3. Measured experimental molal enthalpies of solution ($\Delta_{sol}H^{exp}$) for the dissolution of $Nd(OH)_3$(s) (Eq. 1) in perchloric acid based aqueous solutions from 25 to 150 °C. *I* denotes the ionic strength. Enthalpies measured at an *I* value of 0.01 mol/kg are assumed to be representative for the standard enthalpy of solution ($\Delta_{sol}H°$). Heat flow contributions (q_{obs}, q_{blk}, q_{sol}) are described by Eqs. (2-4). The experimental uncertainty of $\Delta_{sol}H°$ is based on the standard deviation (1σ) of replicate experiments.

T (ºC)	$Nd(OH)_3$(s) (μmol)	q_{obs} (mJ)	q_{blk} (mJ)	q_{sol} (mJ)	$\Delta_{sol}H^{exp}$ (kJ/mol)
	I = 0.01, *T* = 24.23 ±0.01, $\Delta_{sol}H°$ = -146.2 ±0.5 kJ/mol				
24.24	10.14	-1479	-0.8	-1478	-145.7
24.23	9.99	-1459	-0.8	-1458	-145.9
24.22	9.85	-1441	-0.8	-1441	-146.2
24.21	9.84	-1447	-0.8	-1447	-147.0
	I = 0.05, *T* = 24.13 ±0.01, $\Delta_{sol}H^{exp}$ = -143.5 ±3.2 kJ/mol				
24.14	9.92	-1420	-0.8	-1419	-143.0
24.14	9.98	-1467	-0.8	-1466	-146.8
24.12	9.69	-1362	-0.8	-1361	-140.5
	I = 0.09, *T* = 24.13 ±0.01, $\Delta_{sol}H^{exp}$ = -143.4 ±2.7 kJ/mol				
24.22	10.26	-1502	-0.8	-1502	-146.4
24.21	10.26	-1464	-0.8	-1463	-142.6
24.20	10.20	-1439	-0.8	-1439	-141.1
	I = 0.01, *T* = 49.03 ±0.01, $\Delta_{sol}H°$ = -148.7 ±1.6 kJ/mol				
49.03	10.02	-1486	-1.0	-1485	-148.2
49.03	10.05	-1484	-1.0	-1483	-147.5
49.03	9.76	-1470	-1.0	-1469	-150.5
	I = 0.05, *T* = 48.87 ±0.01, $\Delta_{sol}H^{exp}$ = -148.7 ±1.1 kJ/mol				
48.87	9.86	-1477	-1.0	-1476	-149.7
48.87	10.10	-1490	-1.0	-1489	-147.5
48.86	9.76	-1454	-1.0	-1453	-148.9
	I = 0.09, *T* = 48.95 ±0.01, $\Delta_{sol}H^{exp}$ = -145.0 ±3.3 kJ/mol				
48.96	9.86	-1434	-1.0	-1433	-144.1
48.96	10.10	-1475	-1.0	-1474	-142.2
48.95	9.76	-1493	-1.0	-1492	-148.7

Table 3 *(continued)*

T (ºC)	$Nd(OH)_3$(s) (μmol)	q_{obs} (mJ)	q_{blk} (mJ)	q_{sol} (mJ)	$\Delta_{sol}H^{exp}$ (kJ/mol)
I = 0.01, T = 73.84 ±0.01 °C, $\Delta_{sol}H°$ = -146.2 ±1.5 kJ/mol					
73.84	9.90	-1461	-2.1	-1459	-147.3
73.84	9.97	-1443	-2.1	-1441	-144.5
73.84	9.93	-1459	-2.1	-1457	-146.8
I = 0.01, T = 98.72 ±0.08 °C, $\Delta_{sol}H°$ = -149.2 ±1.8 kJ/mol					
98.80	10.21	-1500	-4.3	-1495	-148.2
98.80	10.54	-1503	-4.3	-1498	-147.2
98.74	10.52	-1447	-4.3	-1443	-150.2
98.66	10.38	-1509	-4.3	-1505	-151.7
98.61	9.38	-1433	-4.3	-1428	-148.7
I = 0.01, T = 123.64 ±0.02 °C, $\Delta_{sol}H°$ = -151.7 ±3.0 kJ/mol					
123.64	10.03	-1537	-9.9	-1527	-152.2
123.63	9.80	-1465	-9.9	-1455	-148.5
123.62	9.87	-1533	-9.9	-1524	-154.4
I = 0.01, T = 148.33 ±0.07 °C, $\Delta_{sol}H°$ = -151.5 ±1.8 kJ/mol					
148.36	10.10	-1603	-46.2	-1557	-154.2
148.36	9.86	-1530	-46.2	-1484	-150.5
148.37	9.94	-1559	-46.2	-1513	-152.2
148.38	9.78	-1517	-46.2	-1471	-150.4
148.20	10.39	-1607	-46.2	-1603	-150.2

Table 4. Least squares regression coefficients fitted to the experimental enthalpy of solution ($\Delta_{sol}H°$) values determined in this study as a function of temperature between 25 and 150 °C. Equations (7-10) are used to derive the enthalpy increments [$\Delta_{sol}H°(T)$-$\Delta_{sol}H°(T_r)$], the heat capacity ($\Delta_{sol}C_p°$) and entropy ($\Delta_{sol}S°$) functions.

	Coefficient	$u(a_n)^a$
h_{Tr} [J/mol] · 10^{-3}	-580.8	1.1
a_0 [J/mol·K]	1266.2	8.4
a_1 [J/mol·K^2]	-2.54	0.05
a_2 [J·K/mol] · 10^{-6}	-50.55	0.13

[a] The standard error of the regression is calculated based on the standard deviation (σ), the 95% confidence limit of the regression (U), and the student factor (t) where $\sigma = \sqrt{\frac{\sum^{N}(\Delta_{sol}H^{fit} - \Delta_{sol}H^{exp})^2}{N-1}}$ and $U = t \cdot \sigma$. This calculation made use of the Python Scipy library (Virtanen et al., 2020).

Table 5. Smoothed standard thermodynamic properties of solution for the dissolution of $Nd(OH)_3$(s) according to Eq. (1) calculated from the regressed coefficients in Table 4. The standard Gibbs energy of solution ($\Delta_{sol}G°$) is calculated from Eq. (13).

P (bar)	T (ºC)	$\Delta_{sol}C_p°$ (J/mol·K)	u($\Delta_{sol}C_p°$)[a]	$\Delta_{sol}H°$ (kJ/mol)	$u(\Delta_{sol}H°)$ [b]	$\Delta_{sol}S°$ (J/mol·K)	$u(\Delta_{sol}S°)$[a]	$\Delta_{sol}G°$ (kJ/mol)	$u(\Delta_{sol}G°)$[c]
1.013	25	-58.9	17.0	-146.5	3.5	-127.2	2.2	-108.6	3.6
1.013	50	-37.7	18.1	-147.7	3.9	-131.0	2.6	-105.3	4.0
1.013	75	-34.1	19.2	-148.5	4.3	-133.6	3.6	-102.0	4.5
1.013	100	-43.5	20.3	-149.5	4.8	-136.2	4.7	-98.7	5.1
2.320	125	-62.8	21.4	-150.8	5.3	-139.6	5.9	-95.2	5.8
4.757	150	-89.6	22.5	-152.7	5.8	-144.2	7.2	-91.7	6.5

[a] Uncertainties $u(\Delta_{sol}C_p°)$ and $u(\Delta_{sol}S°)$ are calculated at the 95% confidence limit from Eqs. (10) and (12), respectively, and the error propagation using the parameters listed in Table 4 from the general equation $u(Y) = \sqrt{\sum^{n}(\frac{\partial Y}{\partial a_n})^2 \cdot u^2(a_n)}$; u($Y$) can be u($\Delta_{sol}C_p°$) or u($\Delta_{sol}S°$) and a_n are the parameters of the regression.

[b] Uncertainties $u(\Delta_{sol}H°)$ are calculated at the 95% confidence limit of the regression from Eq. (7).

[c] Uncertainties $u(\Delta_{sol}G°)$ are calculated from the error propagation in Eq. (13), using $u(\Delta_{sol}H°)$ and $u(\Delta_{sol}S°)$.

Table 6. Standard thermodynamic properties of aqueous species at reference conditions (T_r = 25 °C and P_r = 1 bar) and HKF equation of state parameters for extrapolations to high temperature and pressure. Values in bold include the recommended values for the Nd^{3+} aqua ion derived from this experimental study, and where necessary updated for other species.

		$\Delta_f G°_{Tr,Pr}$ (kJ/mol)	$\Delta_f H°_{Tr,Pr}$ (kJ/mol)	$S°_{Tr}$ (J/mol·K)	$C_p°_{Tr}$ (J/mol·K)	$a_1 \cdot 10$ (cal/mol·bar)	$a_2 \cdot 10^{-2}$ (cal/mol)	a_3 (cal·K/bar·mol)	$a_4 \cdot 10^{-4}$ (cal·K/mol)	c_1 (cal/K·mol)	$c_2 \cdot 10^{-4}$ (cal·K/mol)	$\omega \cdot 10^{-5}$ (cal/mol)
Nd^{3+}	This study	**-679.7 ±0.7**	**-704.4 ±0.5**	**-207.1 ±2.2**	**-167.8**							
	Supcrt92	-672.0[b,k]	-696.6 ±1.1[a,k]	-207.1[b,k]	-179.8[f,k]	**-3.37[k]**	**-14.5[k]**	**8.32[k]**	**-2.18[k]**	**1.62[k]**	**-11.8[k]**	**2.26[k]**
		-673.7 ±1.5[d,e]	-694.8 ±2.0[c]									
		-681.7 ±1.0[j]	-706.4[j]									
$Nd(OH)^{2+}$	Supcrt92	-862.7[g,h]	-901.7[g,h]	-13.8[h]	-139.7[h]	2.74[h]	-1.1[h]	6.18[h]	-2.73[h]	-3.21[h]	-9.8[h]	1.11[h]
$Nd(OH)_2^+$	Supcrt92	-811.6[g,h]	-828.1[g,h]	53.13[h]	-315.1[h]	2.83[h]	-0.9[h]	6.1[h]	-2.74[h]	-34.7[h]	-18.4[h]	0.04[h]
$NdCl^{2+}$	This study	**-815.4**	**-895.9**	**-217.2[i]**	**512.9[i]**	**-0.77[i]**	**-9.7[i]**	**9.54[i]**	**-2.38[i]**	**9.33[i]**	**-6.54[i]**	**1.45[i]**
		-807.3[i]	-887.7[i]									
	Supcrt92	-805.0[h]	-849.4[h]	-94.9[h]	-74.89[h]	-0.68[h]	-9.42[h]	9.4[h]	-2.39[h]	8.49[h]	-6.70[h]	1.40[h]
$NdCl_2^+$	This study	**-945.3**	**-1015.4**	**-5.7[i]**	**-144.3[i]**	**2.14[i]**	**-2.55[i]**	**6.75[i]**	**-2.67[i]**	**-8.89[i]**	**-10.1[i]**	**0.56[i]**
		-937.2[i]	-1007.3[i]									
	Supcrt92	-934.7[h]	-1010.4[h]	-24.69[h]	-151.5[h]	2.39[h]	-1.94[h]	6.5[h]	-2.70[h]	-9.18[h]	-10.4[h]	0.64[h]
NdF^{2+}	This study	**-983.6**	**-1016.6**	**-110.8[i]**	**103.5[i]**	**-3.38[i]**	**-16.0[i]**	**12.05[i]**	**-2.12[i]**	**34.2[i]**	**2.00[i]**	**1.49[i]**
		-975.5[i]	-1008.5[i]									
	Supcrt92	-978.6	-1009.18	-61.09	-57.7	-3.33	-+15.9	11.99	-2.12	9.76	-5.87	1.27

[a]Spedding and Miller (1952), solution calorimetry of $NdCl_3$(s) dissolution; [b]Morss (1976), evaluation of experimental thermodynamic properties of solution of $NdCl_3$(s); [c]Cordfunke and Konings (2001a), evaluation of compiled experimental $\Delta_{sol}H°$of $NdCl_3$(s); [d]Wood et al. (2002), $Nd(OH)_3$ solubility experiments; [f]Spedding et al. (1979), electrolysis of $Nd(NO_3)_3$(s); [g]Lee and Byrne (1992), linear free-energy relationships; [h]Haas et al. (1995), estimation of standard partial molal thermodynamic properties using HKF equation of state; [i]Migdisov et al. (2009), REE chloride/fluoride solubility experiments; [j]Pan et al. (2024) from optimization of $\Delta_f G°$ using solubility experimental data of $NdPO_4$(s); [k]Shock et al. (1997), HKF equation of state correlations.

Table 7. Standard thermodynamic properties of Nd solids at reference conditions (T_r = 25 °C and P_r = 1 bar) and heat capacity function (C_p°) function with temperature T in Kelvin. Values in bold are those used and recommended in this study for retrieving the properties of the Nd^{3+} aqua ion.

	$\Delta_f G°_{Tr,Pr}$	$\Delta_f H°_{Tr,Pr}$	$S°_{Tr}$	C_p°	$C_p = a + b\cdot T + c\cdot T^{-2} + d\cdot T^{-1}$			
	(kJ/mol)	(kJ/mol)	(J/mol·K)	(J/mol·K)	a	b ·10^{-2}	c·10^{-3}	d·10^{-3}
$Nd(OH)_3$(s)	**-1283.0 ±2.6**[b,e]	**-1415.6 ±2.3**[a,e]	**117.8 ±0.2**[c]	**117.62 ±0.07**[c]	**174.6**[b]	**1.082**[b]	**983.5**[b]	**-21.24**[b]
	-1270.9 ±1.1[d]	-1403.7 ±1.0[d]						
Nd_2O_3(s)	-1719.8 ±6.6[e]	-1806.9 ±3.0[e,f]	158.7 ±1.0[e]	111.34 ±0.12[e]	117.11[n]	2.814[n]	-1258[n]	
		-1808.1 ±1.0[g]						
		-1807.1 ±3.1[h]						
$NdCl_3$(s)	-965.6[n]	-1029 ±0.9[i]	153.43[n]	99.24[n]	87.28[n]	3.85[n]	40.21[n]	
		-1041.3 ±1.0[j]						
		-1039.5 1.7[l]						
		-1049.9 ±1.0[m,j,l]						
$NdPO_4$(s)	-1846.2[p]	-1965.4[p]	122.9[q]	104.8[q]	132.96[q]	2.254[q]	-3100.9[q]	
	-1849.6[r]	-1968.4[r]						

[a]Merli et al. (1997), solution calorimetry of $Nd(OH)_3$(s), Nd(cr) in 6M HCl; [b]Diakonov et al. (1998a, 1998b), evaluation of experimental thermochemical and solubility data of $Nd(OH)_3$(s); [c]Chirico and Westrum (1981), experimental measurements of heat capacity of $Nd(OH)_3$(s); [d]Morss et al. (1989), solution calorimetry of $Nd(OH)_3$(s) in 6M HCl; [e]Navrotsky et al. (2015), compilation and review of REE solids; [f]Cordfunke and Konings (2001c), compilation and review of experimental data for Nd_2O_3; [g] Huber and Holley (1952), combustion calorimetry of Nd_2O_3(s); [h] Fitzgibbon et al. (1965), solution calorimetry of Nd_2O_3(s) in 2M HCl; [i]Spedding and Miller (1952), solution calorimetry of $NdCl_3$(s); [j]Stuve (1965), solution calorimetry of $NdCl_3$(s); [l]Cordfunke et al. (1996), solution calorimetry of $NdCl_3$(s); [m]Cordfunke and Konings (2001a), compilation and review of experimental data for $NdCl_3$(s); [n]Konings et al. (2014), comprehensive review of the thermodynamic properties; [p]Van Hoozen et al. (2020), solubility experiments of $NdPO_4$(s); [q]Popa et al. (2006), heat capacity of $NdPO_4$(s); [r]Ushakov et al. (2001), calorimetry experiments of $NdPO_4$(s).

Table 8. Least squares regression coefficients fitted to the experimentally derived standard enthalpy of formation ($\Delta_f H°$) values determined in this study as a function of temperature between 25 and 150 °C. Equations (7-10) are used to derive the enthalpy increments [$H°(T)$-$H°(T_r)$] and the heat capacity ($C_p°$) functions.

	Coefficient	$u(a_n)$[a]
h_{Tr} [J/mol] · 10^{-3}	-1146.5	1.1
a_0 [J/mol·K]	1256.0	8.4
a_1 [J/mol·K^2]	-2.68	0.05
a_2 [J·K/mol] · 10^{-6}	-55.56	0.13

[a] The standard error of the regression is calculated based on the standard deviation (σ), the 95% confidence limit of the regression (U), and the student factor (t) where $\sigma = \sqrt{\frac{\sum^N (\Delta_{sol}H^{fit} - \Delta_{sol}H^{exp})^2}{N-1}}$ and $U = t \cdot \sigma$. This calculation made use of the Python Scipy library (Virtanen et al., 2020).

Table 9. Smoothed standard molal thermodynamic properties of formation of Nd^{3+} derived in this study calculated from the regressed coefficients in Table 8. The standard Gibbs energy of formation ($\Delta_f G°$) is calculated from Eq. (16).

P (bar)	T (ºC)	$C_p°$ (J/mol·K)	$u(C_p°)$[a]	$\Delta_f H°$ (kJ/mol)	$u(\Delta_f H°)$[b]	$\Delta_f G°$ (kJ/mol)	$u(\Delta_f G°)$[c]
1.01	25	-167.8	17.0	-704.8	3.5	-680.1	4.7
1.01	50	-141.8	18.1	-708.6	3.9	-674.8	5.1
1.01	75	-135.1	19.2	-712.0	4.3	-669.2	5.5
1.01	100	-142.7	20.2	-715.5	4.8	-663.3	6
2.32	125	-161.2	21.4	-719.2	5.3	-657.2	6.5
4.76	150	-187.9	22.6	-723.6	5.8	-650.8	7

[a] Uncertainties $u(\Delta C_p°)$ is calculated at the 95% confidence limit from Eq. (10) and the error propagation using the parameters listed in Table 8 using the general equation $u(Y) = \sqrt{\sum^n (\frac{\partial Y}{\partial a_n})^2 \cdot u^2(a_n)}$; u($Y$) can be u($\Delta C_p°$) and a_n are the parameters of the regression.

[b] Uncertainties $u(\Delta H°)$ are calculated at the 95% confidence limit of the regression from Eq. (7).

[c] Uncertainties $u(\Delta G°)$ are calculated from the error propagation in Eq. (13), using $u(\Delta H°)$ and $u(\Delta S°)$.

FIGURES

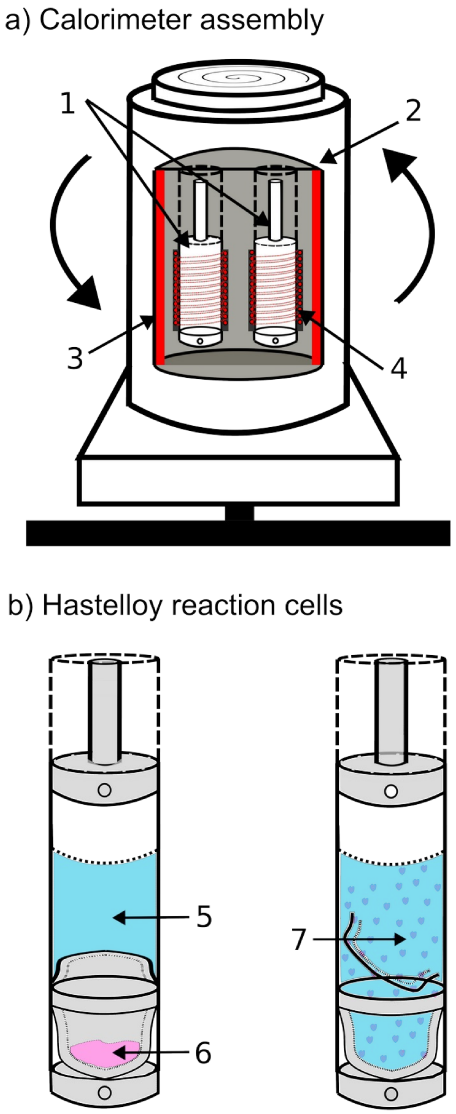

Figure 1: a) Setaram C-80 calorimeter designed for operation up to 10MPa and 300 ºC with rocking mechanism; b) Hastelloy C-276 cell used for dissolution experiments with two isolated compartments for solid and aqueous solution. 1: Reference and sample cells; 2: insulating chamber; 3: heating filament; 4: 3D thermopile fluxmeter; 5: liquid compartment with perchloric acid based experimental starting solutions; 6: Solid compartment with synthetic $Nd(OH)_3(s)$ powder; 7 : Reacted experimental solution after rocking the calorimeter, and opening of liquid and solid compartments.

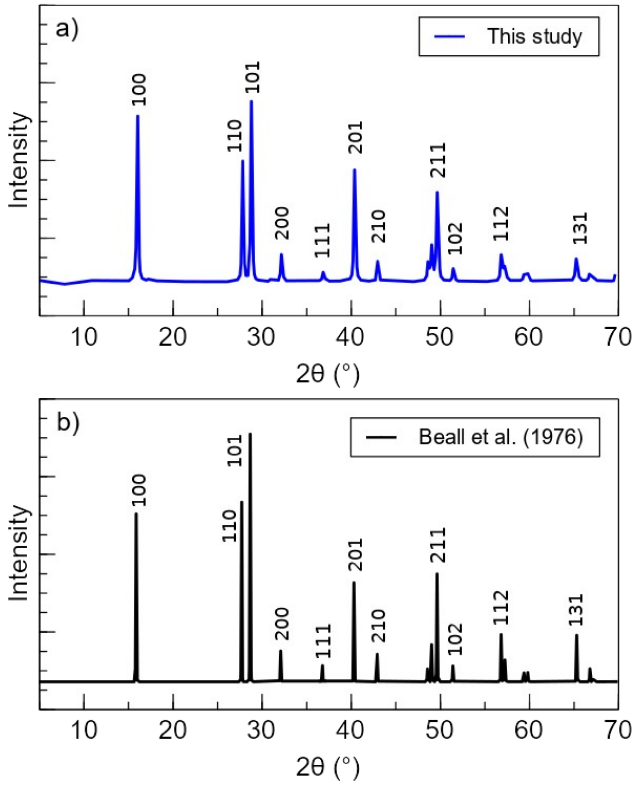

Figure 2: XRD diffraction spectrum of hexagonal ($P6_3/m$) $Nd(OH)_3$(s) a) synthesized hydrothermally at 250 °C in this study, and b) reference spectrum by Beall et al. (1976). Numbers indicate Miller indices for only major XRD peaks. Refined lattice parameters are listed in Table 1.

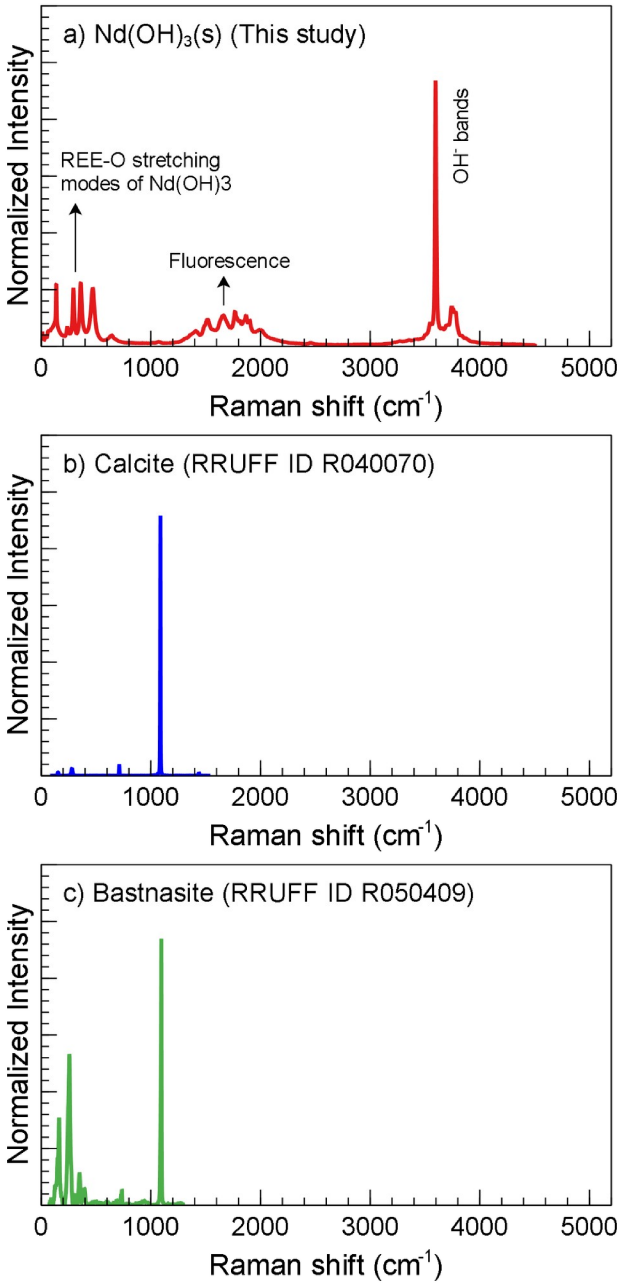

Figure 3: Raman shifts of a) pure $Nd(OH)_3(s)$ synthesized hydrothermally at 250 °C in this study showing REE-O stretching modes of $Nd(OH)_3$ between ~40 and 800 cm^{-1}, fluorescence peaks between 1000 and 2100 cm^{-1}, and OH-bands between 3000 and 3800 cm^{-1}. b-c) Reference Raman spectra for calcite (RRUFF ID R040070) and bastnäsite-(Ce) (RRUFF ID R050409) from the RRUFF database (Lafuente et al., 2015) indicating the location of C-O symmetric stretching bands between 1000 and 1200 cm^{-1}.

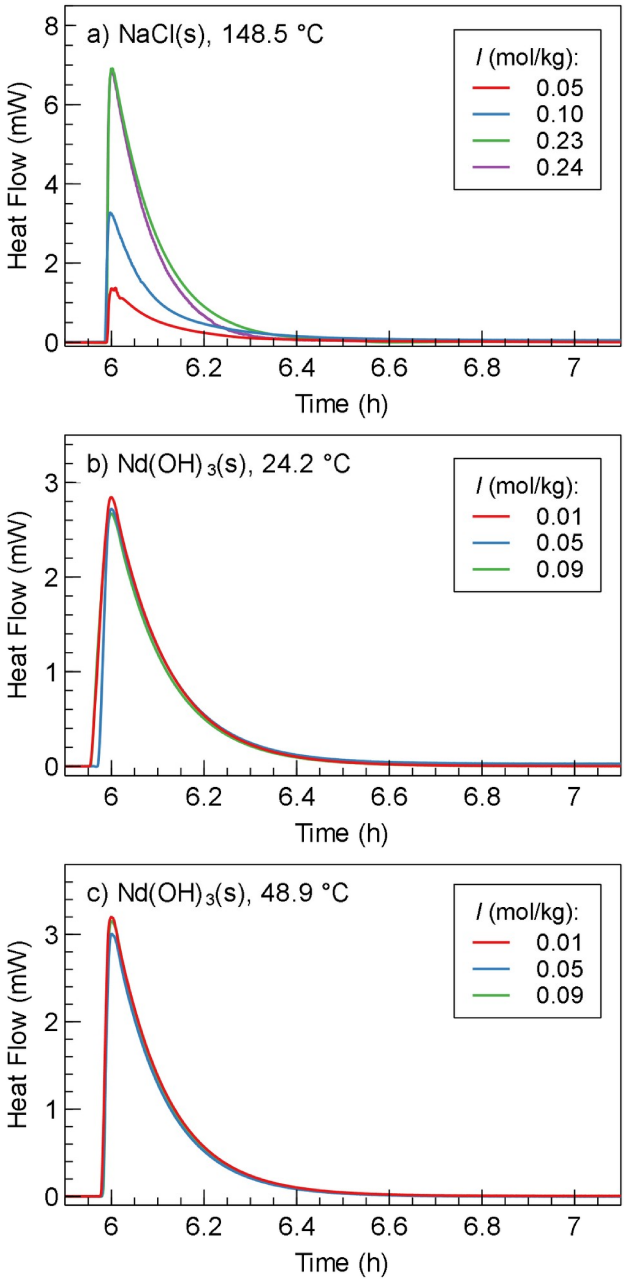

Figure 4: a) Measured heat flow (mW) curves over time (h). a) Dissolution of NaCl(s) at 148.5 °C and varying ionic strength (*I*) from 0.05 to 0.24 mol/kg NaCl. b-c) Dissolution of $Nd(OH)_3$(s) at 24.2 and 48.9 °C with *I* values from 0.01 to 0.09 mol/kg $NaClO_4$. Equilibration time for heat flow curve integration is ~1h. Measured heat flow values are listed in Tables 2 and 3.

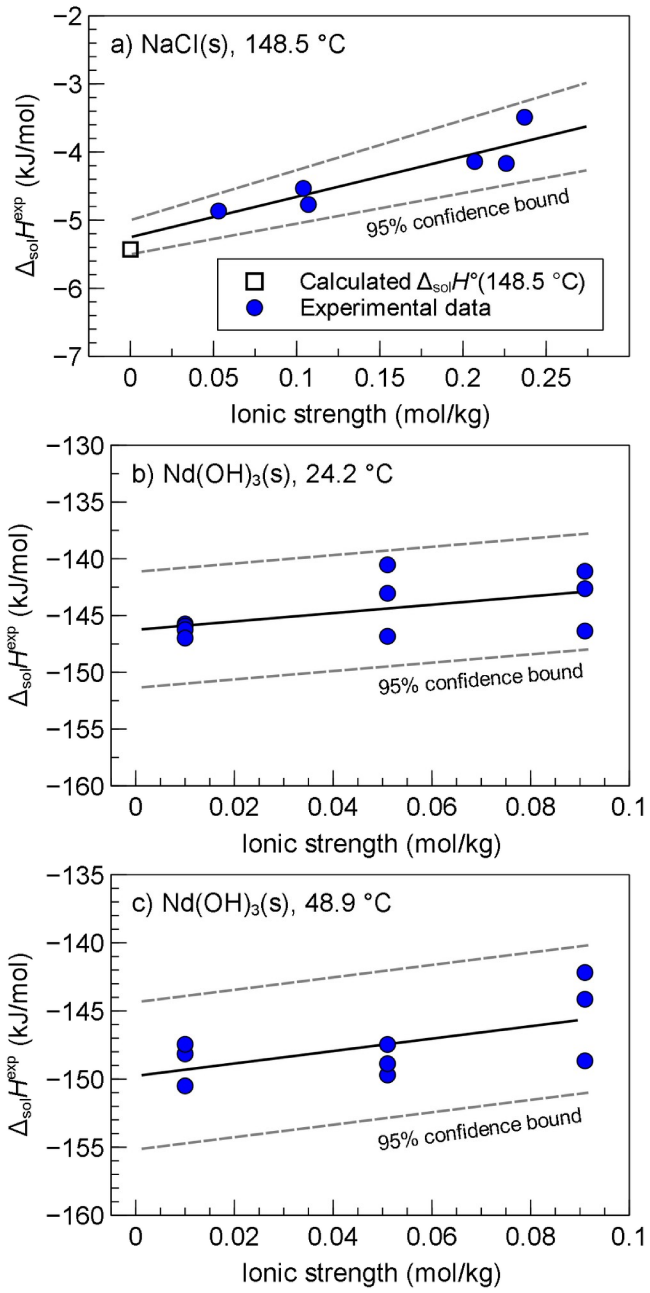

Figure 5: Experimental molal enthalpies of solution ($\Delta_{sol}H^{exp}$ in kJ/mol) as a function of ionic strength (mol/kg) for a) NaCl(s) determined at 148.5 °C in pure water, and b-c) $Nd(OH)_3$(s) measured at 24.2 ºC and 48.9 ºC in perchloric acid/$NaClO_4$ based pH 2 solutions (Table 3). Linear regressions are used for extrapolation to infinite dilution and the standard error of the fits are calculated at the 95% confidence level. The calculated $\Delta_{sol}H°$ value for NaCl was obtained using NaCl(s) from Robie and Hemingway (1995), and aqueous species (Na^+ and Cl^-) from Miron et al. (2016) and Shock and Helgeson (1988).

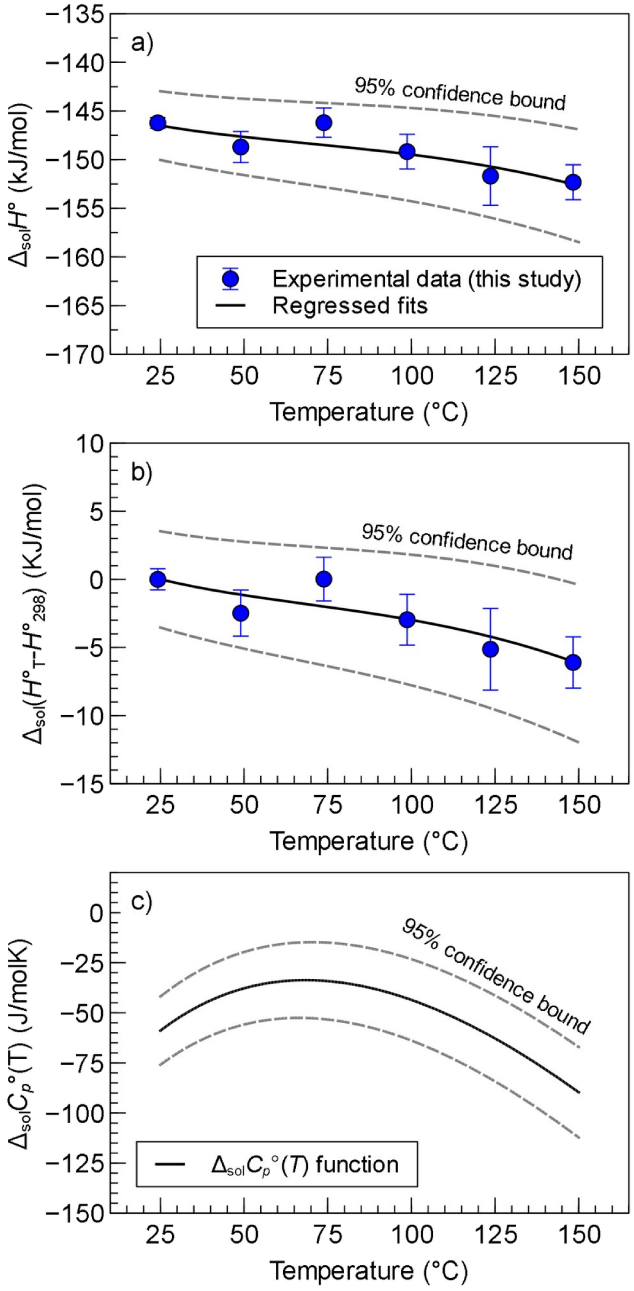

Figure 6: a) Standard enthalpy of solution ($\Delta_{sol}H°$, kJ/mol) for the dissolution of $Nd(OH)_3$(s) determined experimentally as a function of temperature (°C). b) Measured enthalpy increments of solution ($H°_T$- $H°_{298}$, kJ/mol). c) Heat capacity of solution ($\Delta_{sol}C_p°$, J/mol·K) function derived from the measured enthalpy values (Eqs. 9-10). The regressed coefficients, according to Eqs. 7-10, are listed in Table 4 with smoothed values in Table 5.

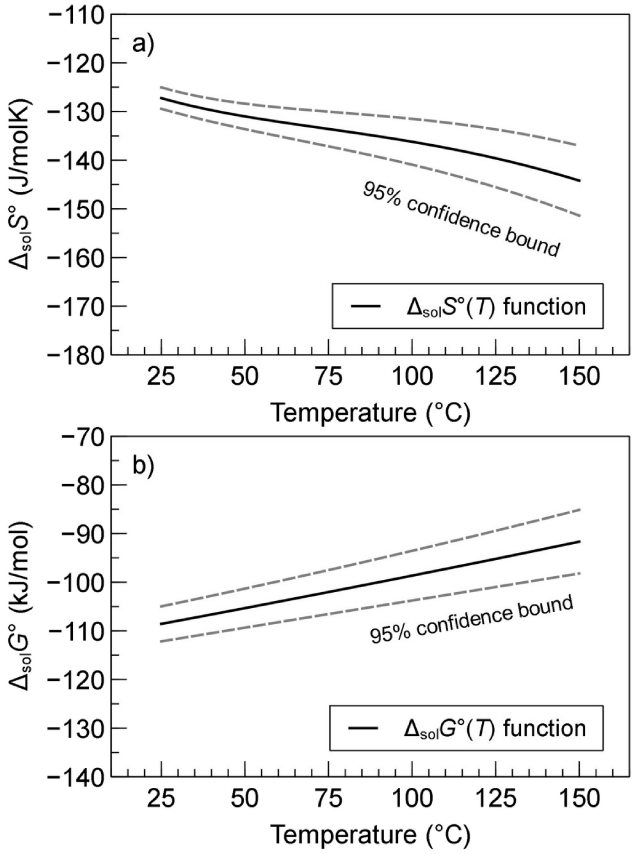

Figure 7: a) Standard entropy of solution ($\Delta_{sol}S°$, J/mol·K) and b) Standard Gibbs energy of solution ($\Delta_{sol}G°$, kJ/mol) as a function of temperature (°C) for the dissolution of $Nd(OH)_3$(s). The entropy is derived from the heat capacity function (Eqs. 11-12). The fitted coefficients are listed in Table 4, and the smoothed values in Table 5.

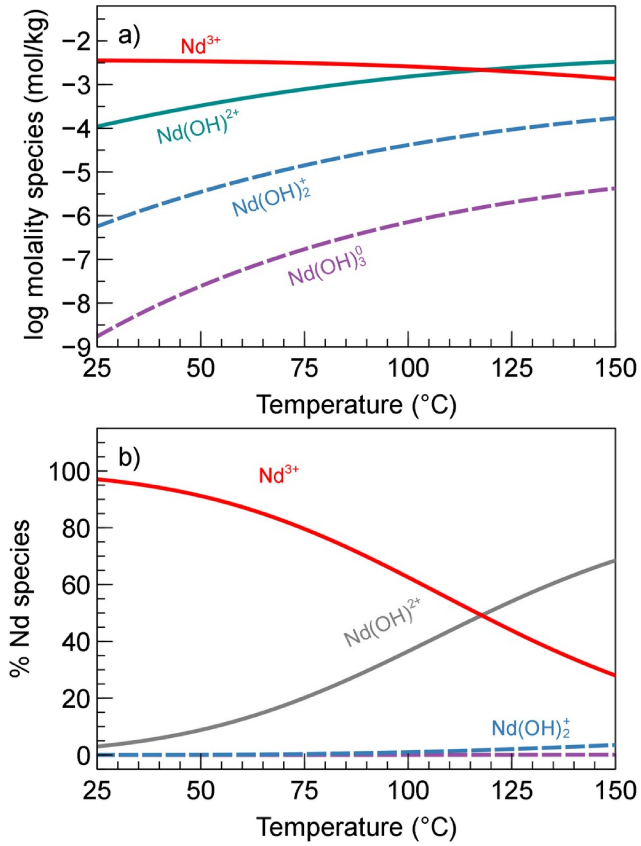

Figure 8: Aqueous speciation calculations showing the predicted stabilities of aqueous Nd species as a function of temperature (°C) for solutions in equilibrium with $Nd(OH)_3(s)$. a) Logarithm molality of the dominant Nd hydroxyl species as a function of temperature modeled using the GEMS code package and the properties of Nd-O-H species listed in Table 6. b) Percent contribution of each aqueous species used for the calculation of modeled enthalpy in Fig. 9.

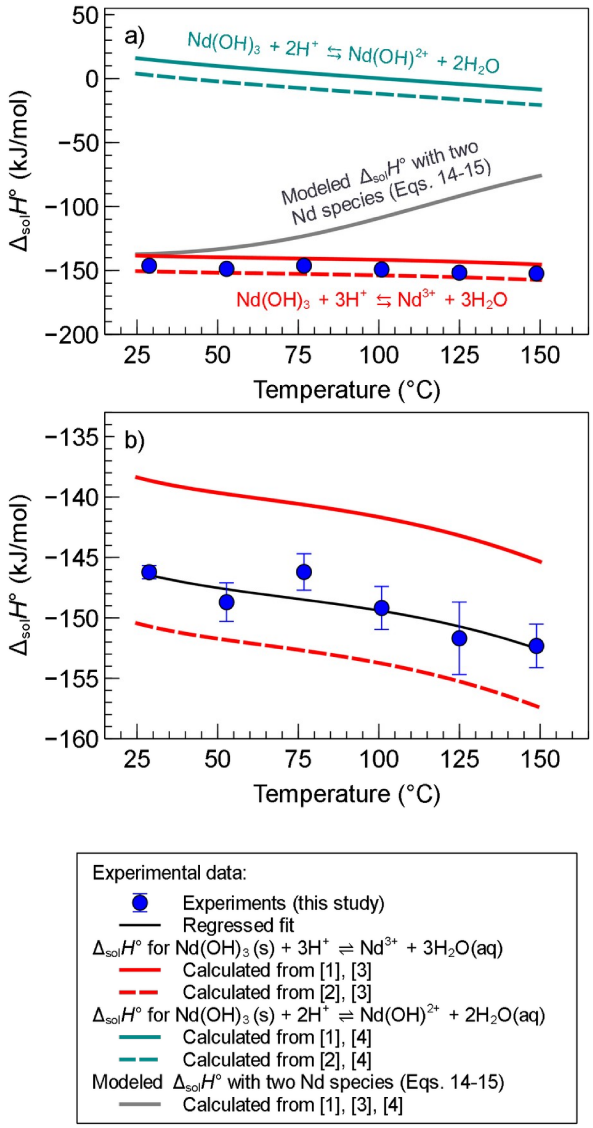

Figure 9: a) Comparison between the measured and predicted enthalpy of solution ($\Delta_{sol}H°$, kJ/mol) as a function of temperature (°C) for individual Nd species participating in Eqs. 14 and and 15. The modeled curve is calculated based on the % contribution of each Nd species at given temperature (Fig. 8). b) Comparison between measured and calculated $\Delta_{sol}H°$ values assuming the Nd^{3+} aqua ion as the main contributing species to the measured enthalpy (Eqs. 1 and 14). References for $\Delta_f H°$ values used in the calculations: [1] $Nd(OH)_3$(s) from Merli et al. (1997); [2] $Nd(OH)_3$(s) from Morss et al. (1989); [3] Nd^{3+} from Shock et al. (1997); [4] $Nd(OH)^{2+}$ from Haas et al. (1995).

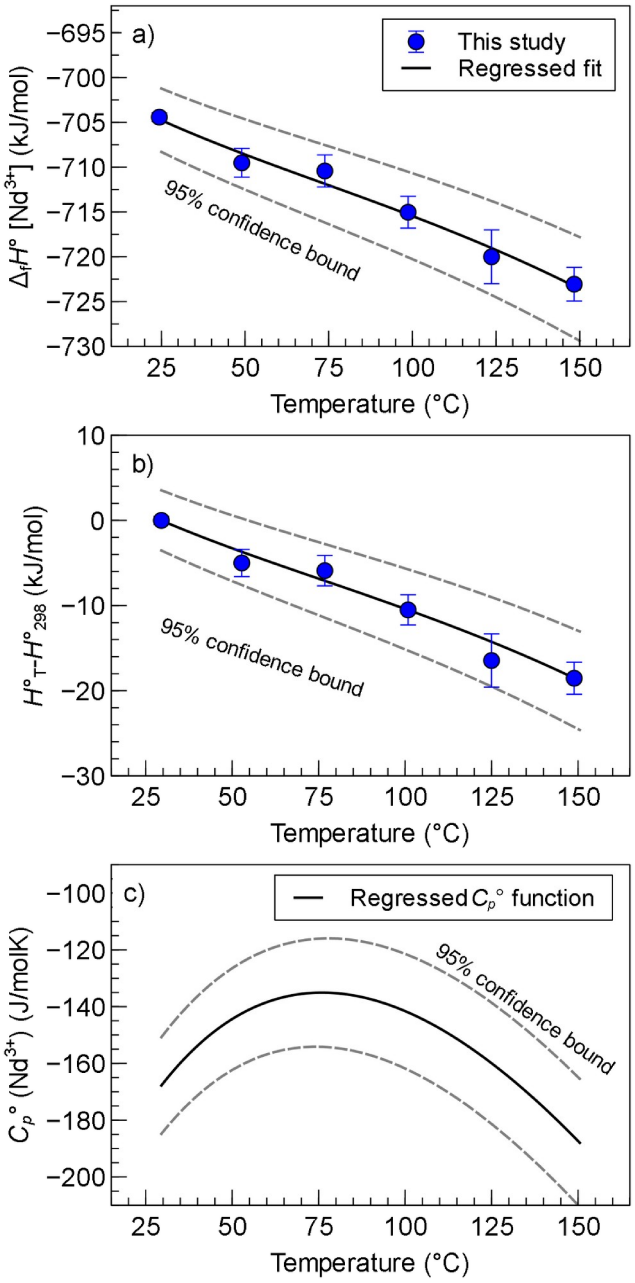

Figure 10: a) Standard partial molal enthalpy of formation ($\Delta_f H°$, kJ/mol) of the Nd^{3+} aqua ion derived according to Eq. 14 from the experimental data from this study and using the $\Delta_f H°$ values for $Nd(OH)_3$(s) from Merli et al. (1997). b) Enthalpy increments ($H°_T$- $H°_{298}$, kJ/mol). c) Heat capacity function ($C_p°$, J/mol·K) derived from the measured enthalpy values (Eqs. 9-10). The regressed coefficients, according to Eqs. 7-10, are listed in Table 8 with smoothed values in Table 9.

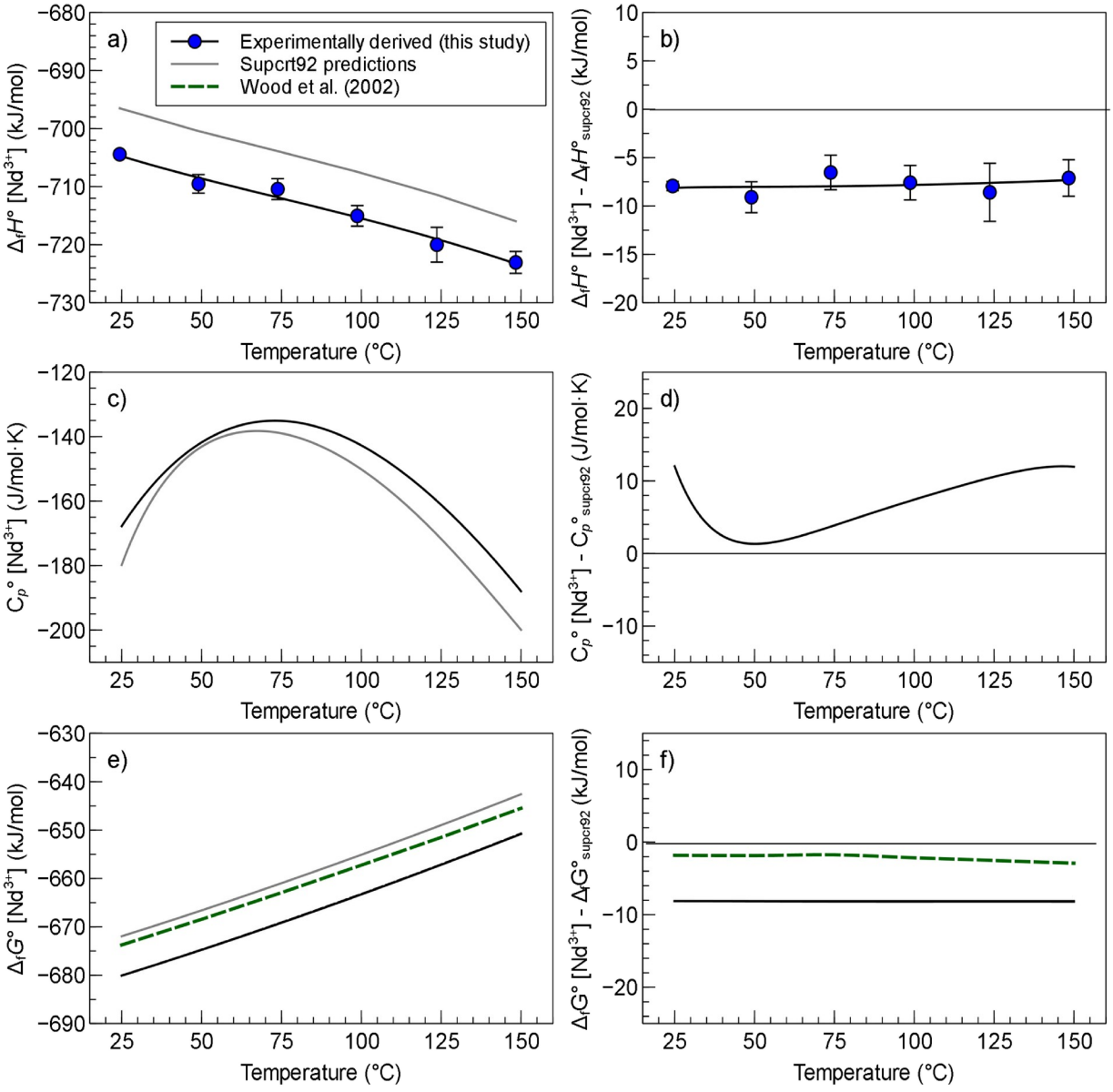

Figure 11: Comparison between the standard partial molal thermodynamic properties of the Nd^{3+} aqua ion determined in this study and predictions from Supcrt92 (Table 6). a) Standard partial molal enthalpy of formation ($\Delta_f H^o$, kJ/mol), c) Standard partial molal heat capacity ($C_p°$, J/mol·K) function, and e) standard partial molal Gibbs of formation ($\Delta_f G^o$, kJ/mol) as a function of temperature (°C). b), d), and f) show the residuals plotted as deviations from predicted values from Supcrt92. The smoothed values are listed in Table 9.

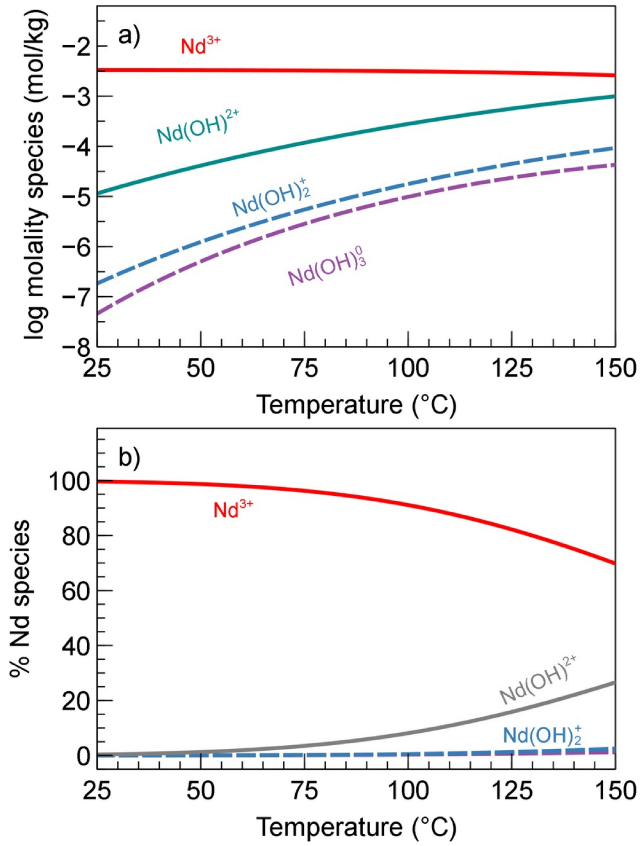

Figure 12: Aqueous speciation calculations using the retrieved $\Delta_f G°$ of Nd^{3+} as a function of temperature (°C) for solutions in equilibrium with $Nd(OH)_3$(s). a) Logarithm molality (mol/kg) of each Nd species as a function of temperature modeled using the GEMS code package and the properties of Nd-O-H species listed in Table 6. b) Percent contribution of each aqueous species.

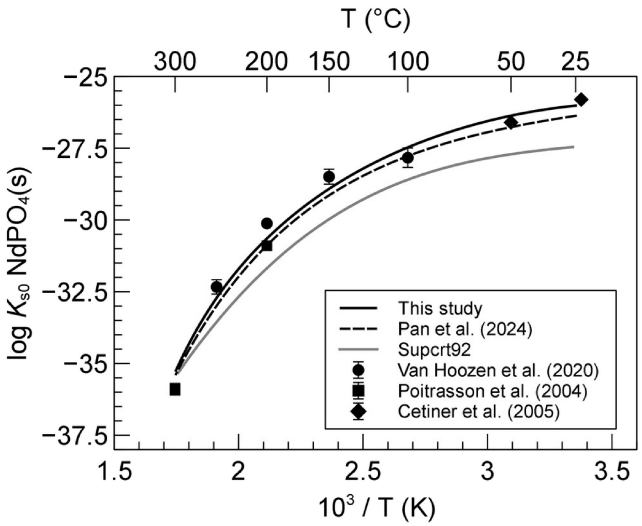

Figure 13: Logarithm of the solubility product (logK_{s0}) of monazite-(Nd) as a function of inverse temperature (10^3/T, in Kelvin), showing a comparison between experimentally derived solubility products (Poitrasson et al., 2004; Cetiner et al., 2005; Van Hoozen et al., 2020), and calculated values using the properties for Nd^{3+} derived in this study, derived from Pan et al. (2024), and those from Supcrt92. The solubility curves were calculated at each temperature using Eqs. (21-22), the properties for Nd^{3+} from Table 6, the properties for $NdPO_4$(s) from Table 7, and the properties for PO_4^{3-} from Shock et al. (1989, 1997).

Supplementary Material

Hydrothermal solution calorimetry in acidic aqueous solutions and revisiting the standard partial molal thermodynamic properties of Nd^{3+} from 25 to 300 °C

Yerko Figueroa Penarrieta*[1,2], Alexander P. Gysi[1,2]

[1] New Mexico Bureau of Geology and Mineral Resources, New Mexico Institute of Mining and Technology, 801 Leroy Place, Socorro, NM 87801, USA

[2] Department of Earth and Environmental Science, New Mexico Institute of Mining and Technology, 801 Leroy Place, Socorro, NM 87801, USA

* Corresponding author: e-mail, yerko.figueroapenarrieta@student.nmt.edu

Tel: +1 575-835-5754

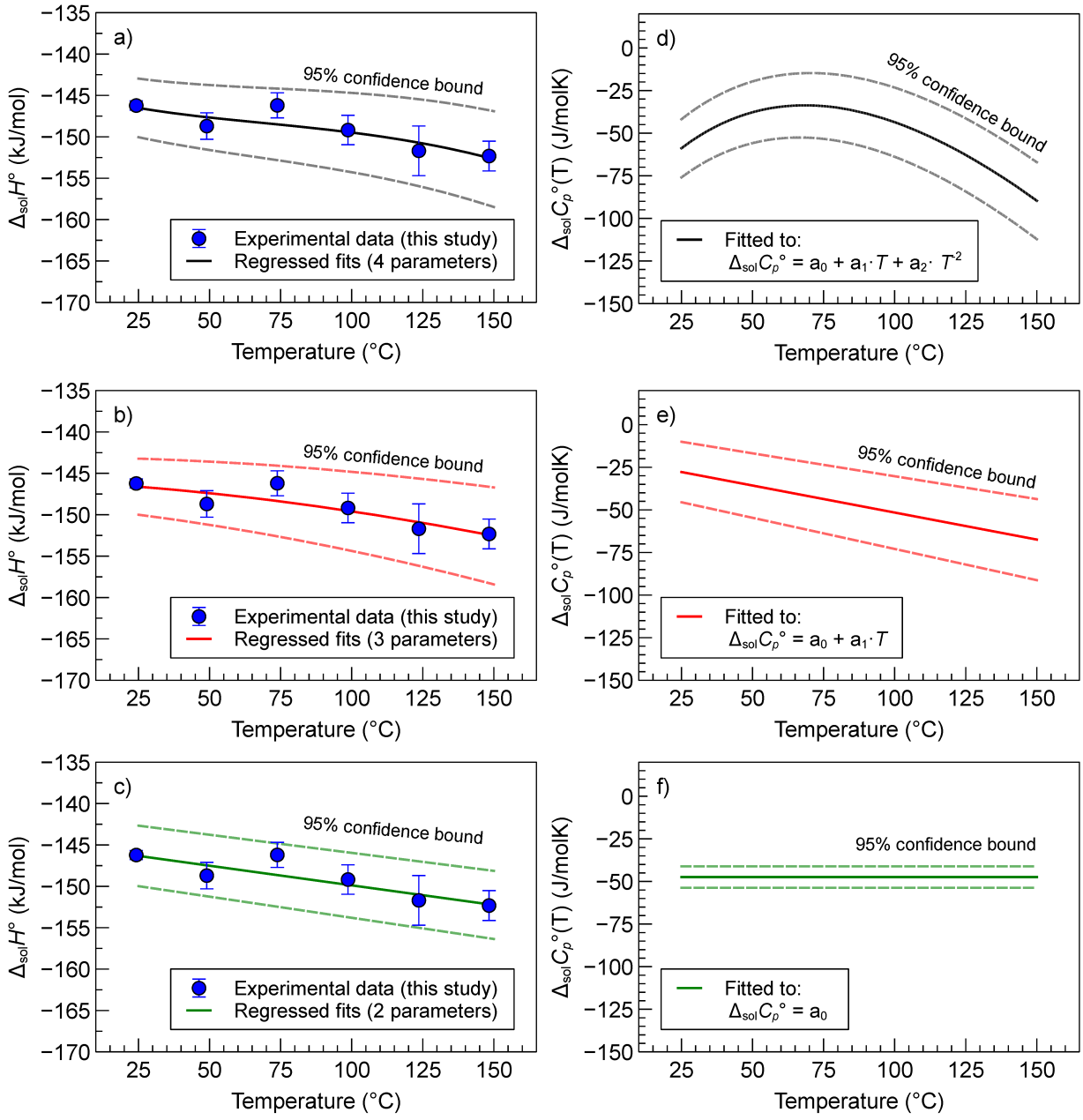

Figure S1. (a-c) Standard enthalpy of solution ($\Delta_{sol}H°$, kJ/mol) for the dissolution of $Nd(OH)_3$(s) determined experimentally as a function of temperature (°C) and (d-f) the resulting heat capacity of solution ($\Delta_{sol}C_p°$, J/mol·K) functions using different fits (Eqs. 7-10). Results from a) and d) show that a four parameter fit (three coefficients a_0-a_2, Tables 4 and 5) reasonably reproduce the expected heat capacity function with an inflection point expected in an aqueous electrolyte (Anderson, 1991).